International Journal of Fracture **126:** 345–384, 2004.

T-stress in orthotropic functionally graded materials: Lekhnitskii and Stroh formalisms

JEONG-HO KIM and GLAUCIO H. PAULINO*
Department of Civil and Environmental Engineering, University of Illinois at Urbana-Champaign, Newmark Laboratory, 205 North Mathews Avenue, Urbana, IL 61801, U.S.A.
**Corresponding Author (E-mail: paulino@uiuc.edu; Phone: (217)333-3817; Fax: (217)265-8041)*

Received 18 November 2002; accepted in revised form 13 January 2004

Abstract. A new interaction integral formulation is developed for evaluating the elastic T-stress for mixed-mode crack problems with arbitrarily oriented straight or curved cracks in orthotropic nonhomogeneous materials. The development includes both the Lekhnitskii and Stroh formalisms. The former is physical and relatively simple, and the latter is mathematically elegant. The gradation of orthotropic material properties is integrated into the element stiffness matrix using a "generalized isoparametric formulation" and (special) graded elements. The specific types of material gradation considered include exponential and hyperbolic-tangent functions, but micromechanics models can also be considered within the scope of the present formulation. This paper investigates several fracture problems to validate the proposed method and also provides numerical solutions, which can be used as benchmark results (e.g. investigation of fracture specimens). The accuracy of results is verified by comparison with analytical solutions.

Key words: functionally graded material (FGM), fracture mechanics, orthotropic materials, T-stress, interaction integral, two-state integral, finite element method (FEM), generalized isoparametric formulation (GIF).

1. Introduction

The non-singular stress (T-stress) of the Williams's eigenfunction expansion (Williams, 1957) influences crack growth under mixed-mode loading (Williams and Ewing, 1972; Ueda et al., 1983; Smith et al., 2001). Williams and Ewing (1972), and Ueda et al. (1983) performed experiments on polymethyl-methacrylate (PMMA) with a slanted internal crack, and found that the elastic T-stress influences the crack initiation angle. Smith et al. (2001) revisited earlier experimental results for brittle fracture of PMMA, and re-examined the role of the T-stress in brittle materials. The T-stress also influences crack path stability for mode I loading with a small imperfection (Cotterell and Rice, 1980).

The T-stress influences crack-tip constraint and toughness under plane strain conditions (see, for example, O'Dowd et al., 1995). Larsson and Carlson (1973) investigated the T-stress, and observed that it affects the size and shape of the plastic zone. Betegón and Hancock (1991) investigated the two-parameter (J-T) characterization of elastic-plastic crack-tip fields. Du and Hancock (1991) investigated the effect of the T-stress on the small-scale yielding field in elastic perfectly-plastic materials. Furthermore, O'Dowd and Shih (1991) developed the J-Q theory (Q is a hydrostatic stress parameter) and found that the Q-family provides a framework for quantifying the evolution of constraint from small-scale yielding to full yielding conditions. They deduced a one-to-one correspondence between Q and T, which is valid in the case where the applied load and geometry affect Q only through T. O'Dowd and Shih (1992)

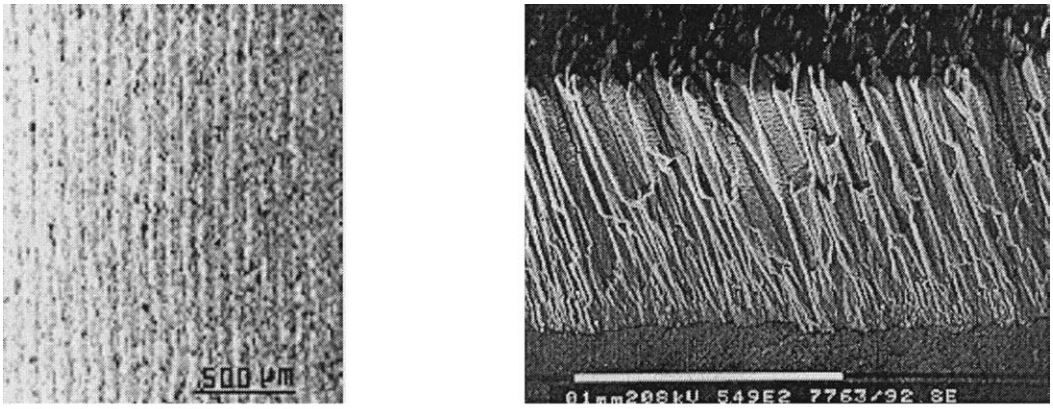

(a) (b)

Figure 1. Cross-section microscope of FGMs: (a) lamellar NiCrAlY-PSZ FGM processed by plasma spray technique (Sampath et al., 1995); (b) columnar $ZrO_2 - Y_2O_3$ thermal barrier coating with graded porosity processed by electron beam physical vapor deposition (Kaysser and Ilschner, 1995).

also showed that the J-Q theory allows toughness to be measured and utilized in engineering applications.

Several numerical methods have been used to evaluate the elastic T-stress. Leevers and Radon (1982) used a variational formulation. Cardew et al. (1985) and Kfouri (1986) used the path-independent J-integral in conjunction with the interaction integral for mode I crack problems. Sladek et al. (1997) used the Betti-Rayleigh reciprocal theorem for mixed-mode crack problems. Recently Chen et al. (2001) investigated the T-stress under mode I loading by means of both the Betti-Rayleigh reciprocal theorem and Eshelby's energy momentum tensor (the path-independent J-integral) using the p-version finite element method (FEM), and addressed the accuracy of numerical computations. All the papers mentioned above are concerned with the T-stress for an isotropic homogeneous material.

The T-stress has been also investigated for both anisotropic and orthotropic homogeneous solids. Gao and Chiu (1992) investigated slightly curved or kinked cracks under mode I loading in orthotropic elastic solids by means of perturbation analysis, which is based on complex variable representations of the Stroh formalism. They also investigated the effects of mode-mixity, material orthotropy, and the T-stress on the behavior of a nearly symmetric crack. Yang and Yuan (2000a) evaluated the elastic T-stress and higher-order coefficients in the crack-tip fields in an anisotropic elastic solid by means of path-independent integrals (J-integral and Betti-Rayleigh reciprocal theorem) and the Stroh formalism. Yang and Yuan (2000b) also investigated a kinked crack in an anisotropic elastic solid, and evaluated the T-stress, stress intensity factors and energy release rates at the main and kinked crack tips by using the integral equation method and the Stroh formalism. However, all of the above papers are concerned with homogeneous materials.

Functionally graded materials (FGMs) possess nonhomogeneous properties. These materials were introduced to benefit from ideal performance of its constituents, e.g. heat and corrosion resistance of ceramics together with mechanical strength and toughness of metals (Illshner, 1996). The books by Suresh and Mortensen (1998) and Miyamoto et al. (1999), and the review chapter by Paulino et al. (2003) present comprehensive information about various

aspects of FGMs. Such materials may exhibit isotropic or orthotropic material properties depending on processing techniques. For instance, large-size bulk FGMs fabricated by the spark plasma sintering (SPS) technique may be modeled as isotropic materials (Tokita, 1999). On the other hand, graded materials processed by plasma spray techniques may have a lamellar structure (Sampath et al., 1995) (see Figure 1a), while materials processed by electron beam physical vapor deposition (PVD) may have a columnar structure (Kaysser and Ilschner, 1995) (see Figure 1b). Thus, an isotropic FGM model can be used for materials fabricated by SPS, and an orthotropic FGM model for materials fabricated by plasma spraying or PVD.

The T-stress has been investigated for isotropic FGMs. Becker et al. (2001) investigated the T-stress and finite crack kinking, and found that the T-stress in FGMs depends on both the far-field loading and the far-field phase angle ($\psi^{\infty} = \tan^{-1}(\sigma_{xy}^{\infty}/\sigma_{yy}^{\infty})$), and that the magnitude of T-stress in the FGMs investigated was, on average, greater than that for homogeneous materials with identical geometry. They calculated the T-stress using the difference of the normal stresses along $\theta = 0$, i.e. $(\sigma_{xx} - \sigma_{yy})$, which is a method that can lead to significant numerical errors due to the recovery of stresses very close to the crack tip. Recently, Kim and Paulino (2003d) proposed a unified approach using the interaction integral method to evaluate T-stress and SIFs, and also investigated the effect of T-stress on the crack initiation angle. In addition, Paulino and Kim (2004) evaluated the T-stress in isotropic FGMs using a non-equilibrium formulation of the interaction integral method, and provided some benchmark solutions for the T-stress and the biaxiality ratio considering graded laboratory fracture specimens. Notice that the papers by Kim and Paulino (2003d) and Paulino and Kim (2004) focus on isotropic FGMs, while the present one focuses on orthotropic FGMs.

The contribution of this paper consists of evaluating the T-stress in orthotropic FGMs by means of the interaction integral method in conjunction with the Lekhnitskii and Stroh formalisms. Based on the assumption that the graded orthotropic material is locally homogeneous near the crack tip, with continuous, differentiable and bounded material properties, this paper establishes the relationship between the asymptotically defined interaction integral (M-integral) and the T-stress, converts the M-integral to an equivalent domain integral (EDI) using auxiliary fields, and calculates the T-stress using a finite domain. This paper builds upon the earlier work by Kim and Paulino (2003b), which focuses on the interaction integral method to evaluate mixed-mode stress intensity factors (SIFs) in orthotropic FGMs.

In this paper, we employ two equivalent formalisms: Lekhnitskii and Stroh, to obtain the auxiliary fields for the T-stress in orthotropic FGMs. The two formalisms treat plane problems in an anisotropic elastic body. While the Lekhnitskii formalism assumes that stress fields depend on plane coordinates, the Stroh formalism assumes that displacement fields depend on plane coordinates. Barnett and Kirchner (1997) provided a direct and straightforward proof of the equivalence between the Lekhnitskii and Stroh formalisms by reducing the six-dimensional form of Stroh's formalism to two homogeneous linear equations, which involve reduced elastic compliances of the Lekhnitskii formalism.

This paper is organized as follows. Section 2 reviews anisotropic elasticity. Section 3 presents the crack-tip fields in anisotropic materials, and Section 4 provides auxiliary fields chosen for the T-stress in the interaction integral method. Section 5 explains the theoretical formulation, and establishes the relationship between the M-integral and the T-stress. Section 6 presents numerical aspects of the M-integral, and various features of the finite element implementation. Section 7 presents various numerical examples. Finally, Section 8 concludes the work.

2. Anisotropic elasticity

The generalized Hooke's law relating stress to strain is given by (Lekhnitskii, 1968)

$$\varepsilon_i = a_{ij}\sigma_j,\ a_{ij} = a_{ji}\ (i, j = 1, 2, \ldots, 6), \tag{1}$$

where the compliance coefficients, a_{ij}, are contracted notations of the compliance tensor S_{ijkl} and the following notation is used

$$\begin{aligned} &\varepsilon_1 = \varepsilon_{11}, \quad \varepsilon_2 = \varepsilon_{22}, \quad \varepsilon_3 = \varepsilon_{33}, \quad \varepsilon_4 = 2\varepsilon_{23}, \quad \varepsilon_5 = 2\varepsilon_{13}, \quad \varepsilon_6 = 2\varepsilon_{12} \\ &\sigma_1 = \sigma_{11}, \quad \sigma_2 = \sigma_{22}, \quad \sigma_3 = \sigma_{33}, \quad \sigma_4 = \sigma_{23}, \quad \sigma_5 = \sigma_{13}, \quad \sigma_6 = \sigma_{12}. \end{aligned} \tag{2}$$

For plane stress, the a_{ij} components of interest are

$$a_{ij}\ \ (i, j = 1, 2, 6) \tag{3}$$

and for plane strain, a_{ij} are exchanged with b_{ij} as follows:

$$b_{ij} = a_{ij} - \frac{a_{i3}a_{j3}}{a_{33}}\ (i, j = 1, 2, 6). \tag{4}$$

Two dimensional anisotropic elasticity problems can be formulated in terms of the analytic functions, $\phi_k(z_k)$, of the complex variable, $z_k = x_k + iy_k\ (k = 1, 2)$, $i = \sqrt{-1}$, where

$$x_k = x + \alpha_k y, \quad y_k = \beta_k y,\ (k = 1, 2). \tag{5}$$

The parameters α_k and β_k are the real and imaginary parts of $\mu_k = \alpha_k + i\beta_k$, which can be determined from the following characteristic equation (Lekhnitskii, 1968)

$$a_{11}\mu^4 - 2a_{16}\mu^3 + (2a_{12} + a_{66})\mu^2 - 2a_{26}\mu + a_{22} = 0, \tag{6}$$

where the roots μ_k are always complex or purely imaginary in conjugate pairs as $\mu_1, \overline{\mu_1}; \mu_2, \overline{\mu_2}$.

3. Crack-tip fields: actual fields

Figure 2 shows Cartesian and polar coordinate systems originating at a crack tip in an orthotropic FGM. The asymptotic stress and displacement fields are given by (see Sih et al. (1965) for the homogeneous case)

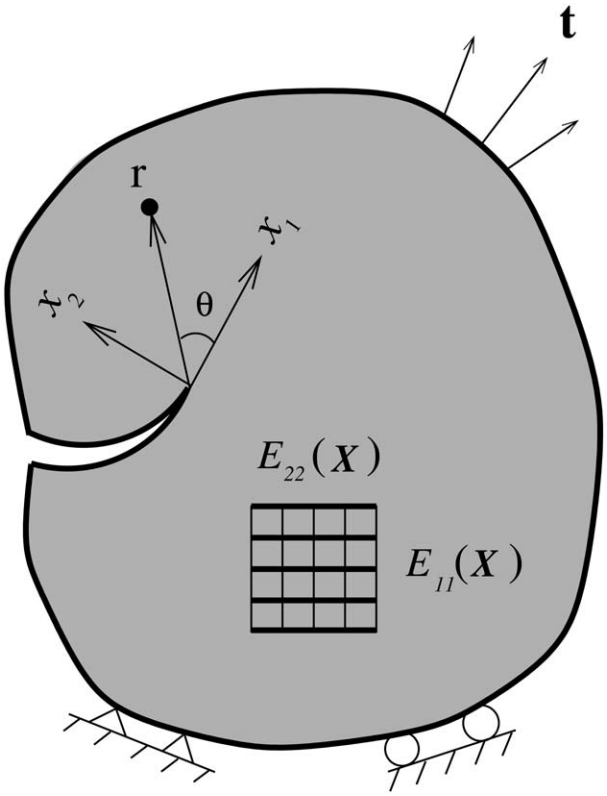

Figure 2. Cartesian (x_1, x_2) and polar (r, θ) coordinates originating from a crack tip in an orthotropic nonhomogeneous material under traction (**t**) and displacement boundary conditions.

$$
\begin{aligned}
\sigma_{11} &= \frac{K_I}{\sqrt{2\pi r}}\,\mathrm{Re}\left[\frac{\mu_1^{\mathrm{tip}}\mu_2^{\mathrm{tip}}}{\mu_1^{\mathrm{tip}}-\mu_2^{\mathrm{tip}}}\left\{\frac{\mu_2^{\mathrm{tip}}}{\sqrt{\cos\theta+\mu_2^{\mathrm{tip}}\sin\theta}}-\frac{\mu_1^{\mathrm{tip}}}{\sqrt{\cos\theta+\mu_1^{\mathrm{tip}}\sin\theta}}\right\}\right]\\
&\quad+\frac{K_{II}}{\sqrt{2\pi r}}\,\mathrm{Re}\left[\frac{1}{\mu_1^{\mathrm{tip}}-\mu_2^{\mathrm{tip}}}\left\{\frac{(\mu_2^{\mathrm{tip}})^2}{\sqrt{\cos\theta+\mu_2^{\mathrm{tip}}\sin\theta}}-\frac{(\mu_1^{\mathrm{tip}})^2}{\sqrt{\cos\theta+\mu_1^{\mathrm{tip}}\sin\theta}}\right\}\right]+T,\\
\sigma_{22} &= \frac{K_I}{\sqrt{2\pi r}}\,\mathrm{Re}\left[\frac{1}{\mu_1^{\mathrm{tip}}-\mu_2^{\mathrm{tip}}}\left\{\frac{\mu_1^{\mathrm{tip}}}{\sqrt{\cos\theta+\mu_2^{\mathrm{tip}}\sin\theta}}-\frac{\mu_2^{\mathrm{tip}}}{\sqrt{\cos\theta+\mu_1^{\mathrm{tip}}\sin\theta}}\right\}\right]\\
&\quad+\frac{K_{II}}{\sqrt{2\pi r}}\,\mathrm{Re}\left[\frac{1}{\mu_1^{\mathrm{tip}}-\mu_2^{\mathrm{tip}}}\left\{\frac{1}{\sqrt{\cos\theta+\mu_2^{\mathrm{tip}}\sin\theta}}-\frac{1}{\sqrt{\cos\theta+\mu_1^{\mathrm{tip}}\sin\theta}}\right\}\right],\\
\sigma_{12} &= \frac{K_I}{\sqrt{2\pi r}}\,\mathrm{Re}\left[\frac{\mu_1^{\mathrm{tip}}\mu_2^{\mathrm{tip}}}{\mu_1^{\mathrm{tip}}-\mu_2^{\mathrm{tip}}}\left\{\frac{1}{\sqrt{\cos\theta+\mu_1^{\mathrm{tip}}\sin\theta}}-\frac{1}{\sqrt{\cos\theta+\mu_2^{\mathrm{tip}}\sin\theta}}\right\}\right]\\
&\quad+\frac{K_{II}}{\sqrt{2\pi r}}\,\mathrm{Re}\left[\frac{1}{\mu_1^{\mathrm{tip}}-\mu_2^{\mathrm{tip}}}\left\{\frac{\mu_1^{\mathrm{tip}}}{\sqrt{\cos\theta+\mu_1^{\mathrm{tip}}\sin\theta}}-\frac{\mu_2^{\mathrm{tip}}}{\sqrt{\cos\theta+\mu_2^{\mathrm{tip}}\sin\theta}}\right\}\right],
\end{aligned}
\tag{7}
$$

and

$$
\begin{aligned}
u_1 &= K_I\sqrt{\frac{2r}{\pi}}\mathrm{Re}\left[\frac{1}{\mu_1^{\mathrm{tip}}-\mu_2^{\mathrm{tip}}}\left\{\mu_1^{\mathrm{tip}}p_2^{\mathrm{tip}}\sqrt{\cos\theta+\mu_2^{\mathrm{tip}}\sin\theta}-\mu_2^{\mathrm{tip}}p_1^{\mathrm{tip}}\sqrt{\cos\theta+\mu_1^{\mathrm{tip}}\sin\theta}\right\}\right] \\
&+ K_{II}\sqrt{\frac{2r}{\pi}}\mathrm{Re}\left[\frac{1}{\mu_1^{\mathrm{tip}}-\mu_2^{\mathrm{tip}}}\left\{p_2^{\mathrm{tip}}\sqrt{\cos\theta+\mu_2^{\mathrm{tip}}\sin\theta}-p_1^{\mathrm{tip}}\sqrt{\cos\theta+\mu_1^{\mathrm{tip}}\sin\theta}\right\}\right]+a_{11}^{\mathrm{tip}}Tr\cos\theta, \\
u_2 &= K_I\sqrt{\frac{2r}{\pi}}\mathrm{Re}\left[\frac{1}{\mu_1^{\mathrm{tip}}-\mu_2^{\mathrm{tip}}}\left\{\mu_1^{\mathrm{tip}}q_2^{\mathrm{tip}}\sqrt{\cos\theta+\mu_2^{\mathrm{tip}}\sin\theta}-\mu_2^{\mathrm{tip}}q_1^{\mathrm{tip}}\sqrt{\cos\theta+\mu_1^{\mathrm{tip}}\sin\theta}\right\}\right] \\
&+ K_{II}\sqrt{\frac{2r}{\pi}}\mathrm{Re}\left[\frac{1}{\mu_1^{\mathrm{tip}}-\mu_2^{\mathrm{tip}}}\left\{q_2^{\mathrm{tip}}\sqrt{\cos\theta+\mu_2^{\mathrm{tip}}\sin\theta}-q_1^{\mathrm{tip}}\sqrt{\cos\theta+\mu_1^{\mathrm{tip}}\sin\theta}\right\}\right]+a_{12}^{\mathrm{tip}}Tr\sin\theta,
\end{aligned}
\tag{8}
$$

respectively, where T denotes the elastic T-stress, a_{11}^{tip} and a_{12}^{tip} denote material parameters evaluated at the crack tip, Re denotes the real part of the complex function, and μ_1^{tip} and μ_2^{tip} denote crack-tip material parameters evaluated by means of Equation (6), which are taken for $\beta_k > 0$ $(k = 1, 2)$, and p_k^{tip} and q_k^{tip} are given by

$$
\begin{aligned}
p_k^{\mathrm{tip}} &= a_{11}^{\mathrm{tip}}(\mu_k^{\mathrm{tip}})^2 + a_{12}^{\mathrm{tip}} - a_{16}^{\mathrm{tip}}\mu_k^{\mathrm{tip}}, \\
q_k^{\mathrm{tip}} &= a_{12}^{\mathrm{tip}}\mu_k^{\mathrm{tip}} + \frac{a_{22}^{\mathrm{tip}}}{\mu_k^{\mathrm{tip}}} - a_{26}^{\mathrm{tip}},
\end{aligned}
\tag{9}
$$

respectively. Notice that in the above expressions, the material parameters are sampled at the crack-tip location, which is the main difference from the expressions for homogeneous materials (Sih et al., 1965).

4. Auxiliary fields

Auxiliary fields are secondary field solutions. Superposition of auxiliary and actual fields leads to the relationship between the interaction integral and the target solution (T-stress). The auxiliary fields involve stresses ($\boldsymbol{\sigma}^{aux}$), strains ($\boldsymbol{\varepsilon}^{aux}$) and displacements ($\boldsymbol{u}^{aux}$). In this paper, we adopt fields (stresses and displacements) originally developed for homogeneous materials and use a formulation (Kim and Paulino, 2003a, 2003d) which accounts for the displacement mismatch between the homogeneous and graded materials.

4.1. Stress and Displacement Fields

To evaluate the T-stress, we use the auxiliary fields associated with a point force applied to the crack tip of a semi-infinite crack in an infinite *homogeneous orthotropic* body in a direction parallel to the crack surface, as illustrated in Figure 3. The material orthotropy directions are aligned with the global coordinates. The auxiliary fields are derived by means of the equivalent Lekhnitskii and Stroh formalisms, which are explained below (see also Kim (2003)).

4.1.1. *Lekhnitskii Formalism*

The Lekhnitskii formalism generalizes the Muskhelishvili approach (Muskhelishvili, 1933) for two-dimensional deformation of an anisotropic elastic body, and begins with stresses by assuming that they only depend on plane coordinates. Details are explained in the book by

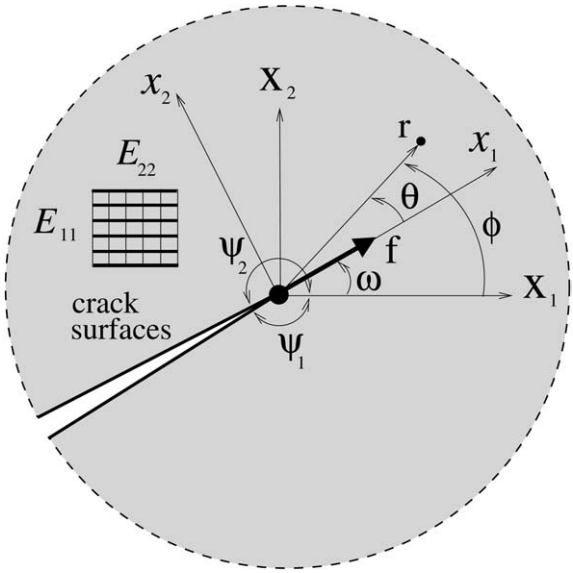

Figure 3. A point force applied at the crack tip in the direction parallel to the crack surface in a homogeneous orthotropic body where material orthotropy directions are aligned with the global coordinates.

Ting (1996). In the Lekhnitskii formalism, we use the known auxiliary stress fields, and determine derivatives of auxiliary displacements. The auxiliary stresses, with respect to the polar coordinates (r, ϕ), are given as (Lekhnitskii, 1968):

$$\sigma_{rr}^{aux} = \frac{A\cos\phi + B\sin\phi}{r\mathcal{F}(\phi)}, \quad \sigma_{\phi\phi}^{aux} = \sigma_{r\phi}^{aux} = 0, \tag{10}$$

where

$$\mathcal{F}(\phi) = a_{11}^{\text{tip}}\cos^4\phi + (2a_{12}^{\text{tip}} + a_{66}^{\text{tip}})\sin^2\phi\cos^2\phi + a_{22}^{\text{tip}}\sin^4\phi \tag{11}$$

and the material parameters $a_{ij} \equiv a_{ij}^{\text{tip}}$ are evaluated at the crack tip location, which differ from a homogeneous material (Lekhnitskii, 1968). The constants A and B are determined from equilibrium conditions for a semi-infinite crack in an infinite homogeneous orthotropic body as shown in Figure 3. The equilibrium equations with respect to the global Cartesian coordinates, i.e. X_1 and X_2, are (Lekhnitskii, 1968)

$$\begin{aligned} A\int_{-\psi_1}^{\psi_2}\frac{\cos^2\phi}{\mathcal{F}(\phi)}d\phi + B\int_{-\psi_1}^{\psi_2}\frac{\sin\phi\,\cos\phi}{\mathcal{F}(\phi)}d\phi &= -f\cos\omega, \\ A\int_{-\psi_1}^{\psi_2}\frac{\sin\phi\,\cos\phi}{\mathcal{F}(\phi)}d\phi + B\int_{-\psi_1}^{\psi_2}\frac{\sin^2\phi}{\mathcal{F}(\phi)}d\phi &= -f\sin\omega. \end{aligned} \tag{12}$$

The auxiliary stresses with respect to the global coordinates are given by

$$\begin{aligned} \sigma_{11}^{aux} &= \frac{A\cos\phi + B\sin\phi}{r\mathcal{F}(\phi)}\cos^2\phi, \\ \sigma_{22}^{aux} &= \frac{A\cos\phi + B\sin\phi}{r\mathcal{F}(\phi)}\sin^2\phi, \\ \sigma_{12}^{aux} &= \frac{A\cos\phi + B\sin\phi}{r\mathcal{F}(\phi)}\sin\phi\cos\phi. \end{aligned} \tag{13}$$

Using the stress-strain and strain-displacement relationships, one obtains displacement derivatives with respect to the global Cartesian coordinates as follows:

$$\begin{aligned}
u_{1,1} &= (a_{11}^{\text{tip}}\cos^2\phi + a_{12}^{\text{tip}}\sin^2\phi)\frac{A\cos\phi + B\sin\phi}{r\mathcal{F}(\phi)},\\
u_{2,2} &= (a_{12}^{\text{tip}}\cos^2\phi + a_{22}^{\text{tip}}\sin^2\phi)\frac{A\cos\phi + B\sin\phi}{r\mathcal{F}(\phi)},\\
u_{1,2} &= \frac{1}{r\mathcal{F}(\phi)}\{A\sin\phi\mathcal{F}(\phi) - A\mathcal{H}_1(\phi) - B\mathcal{H}_2(\phi)\},\\
u_{2,1} &= \frac{1}{r\mathcal{F}(\phi)}[2a_{66}^{\text{tip}}(A\cos\phi + B\sin\phi)\sin\phi\cos\phi - \{A\sin\phi\mathcal{F}(\phi) - A\mathcal{H}_1(\phi) - B\mathcal{H}_2(\phi)\}],
\end{aligned} \tag{14}$$

where

$$\begin{aligned}
\mathcal{H}_1(\phi) &= a_{11}^{\text{tip}}\cos^4\phi\sin\phi + a_{12}^{\text{tip}}\sin\phi\cos^2\phi - a_{22}^{\text{tip}}\sin^3\phi\cos^2\phi - (2a_{12}^{\text{tip}} + a_{66}^{\text{tip}})\sin\phi\cos^4\phi,\\
\mathcal{H}_2(\phi) &= a_{11}^{\text{tip}}\cos^3\phi + a_{12}^{\text{tip}}\sin^2\phi\cos\phi.
\end{aligned} \tag{15}$$

The actual derivation of Equation (14) is given in Appendix A.

4.1.2. *Stroh Formalism*

The Stroh formalism considers two-dimensional deformation of an anisotropic elastic body, and starts with displacements by assuming that they only depend on plane coordinates. Details are explained in the book by Ting (1996). In the Stroh formalism, the auxiliary displacements with respect to the local coordinates (x_1, x_2) are given by (Ting, 1996):

$$\boldsymbol{u}^{aux} = -\frac{1}{2}\left[\frac{1}{\pi}\ln r\boldsymbol{I} + \boldsymbol{S}(\theta)\right]\boldsymbol{h}, \tag{16}$$

where $\boldsymbol{u}^{aux}$=$[u_1^{aux}, u_2^{aux}]^T$, $\boldsymbol{I}$ denotes the identity matrix, and $\boldsymbol{S}(\theta)$ and $\boldsymbol{h}$ are given by

$$\begin{aligned}
\boldsymbol{S}(\theta) &= \frac{2}{\pi}\,\text{Re}\,[\boldsymbol{A}\,\boldsymbol{C}(\theta)\,\boldsymbol{B}^T],\\
\boldsymbol{h} &= \boldsymbol{L}^{-1}\boldsymbol{f},
\end{aligned} \tag{17}$$

where

$$\begin{aligned}
&\boldsymbol{A} = \begin{bmatrix} \lambda_1^{\text{tip}}p_1^{\text{tip}} & \lambda_2^{\text{tip}}p_2^{\text{tip}} \\ \lambda_1^{\text{tip}}q_1^{\text{tip}} & \lambda_2^{\text{tip}}q_2^{\text{tip}} \end{bmatrix}, \quad \boldsymbol{B} = \begin{bmatrix} -\lambda_1^{\text{tip}}\mu_1^{\text{tip}} & -\lambda_2^{\text{tip}}\mu_2^{\text{tip}} \\ \lambda_1^{\text{tip}} & \lambda_2^{\text{tip}} \end{bmatrix},\\
&\boldsymbol{C}(\theta) = \begin{bmatrix} \ln s_1(\theta) & 0 \\ 0 & \ln s_2(\theta) \end{bmatrix}, \quad s_k(\theta) = \cos\theta + \mu_k^{\text{tip}}\sin\theta,\\
&\boldsymbol{L}^{-1} = \text{Re}\,[i\boldsymbol{A}\boldsymbol{B}^{-1}], \quad \boldsymbol{f} = [f, 0]^T,
\end{aligned} \tag{18}$$

in which p_k^{tip} and q_k^{tip} $(k = 1, 2)$ are given by Equation (9), and λ_k^{tip} $(k = 1, 2)$ is the normalization factor given by the following expression

$$2(\lambda_k^{\text{tip}})^2(q_k^{\text{tip}}/\mu_k^{\text{tip}} - \mu_k^{\text{tip}}p_k^{\text{tip}}) = 1. \tag{19}$$

The auxiliary stresses, with respect to the local Cartesian coordinates (x_1, x_2), are given by (Ting, 1996) $(k = 1, 2)$:

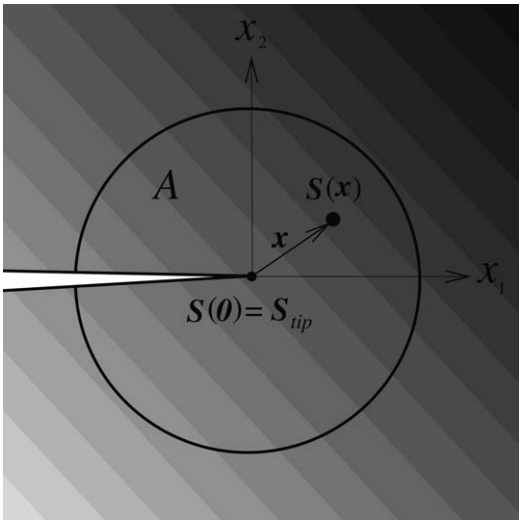

Figure 4. Illustration of the 'incompatibility formulation' accounting for material nonhomogeneity. Notice that $\boldsymbol{S}(\boldsymbol{x}) \neq \boldsymbol{S}_{tip}$ for $\boldsymbol{x} \neq \boldsymbol{0}$. The area A denotes a representative region around the crack tip.

$$\sigma_{rr}^{aux} = \frac{1}{2\pi r}\boldsymbol{n}^T(\theta)\boldsymbol{N}_3(\theta)\boldsymbol{h}, \quad \sigma_{\theta\theta}^{aux} = \sigma_{r\theta}^{aux} = 0, \tag{20}$$

where

$$\boldsymbol{n} = [\cos\theta, \sin\theta]^T, \quad \boldsymbol{N}_3(\theta) = 2\mathrm{Re}\,[\boldsymbol{B}\ \boldsymbol{P}(\theta)\ \boldsymbol{B}^T]$$

$$\boldsymbol{P}(\theta) = \begin{bmatrix} \mu_1(\theta) & 0 \\ 0 & \mu_2(\theta) \end{bmatrix}, \mu_k(\theta) = \frac{\mu_k^{\mathrm{tip}}\cos\theta - \sin\theta}{\mu_k^{\mathrm{tip}}\sin\theta + \cos\theta}. \tag{21}$$

In Equations (16) to (21), material parameters are evaluated at the crack tip location, which differs from a homogeneous material (Yang and Yuan, 2000a). Further details of the Stroh formalism are given in Appendix B.

4.2. Strain Field

In this paper, we use an 'incompatibility formulation' that involves the auxiliary strain field given by

$$\varepsilon_{ij}^{aux} = S_{ijkl}(\boldsymbol{x})\,\sigma_{kl}^{aux}, \tag{22}$$

where $S_{ijkl}(\boldsymbol{x})$ is the compliance tensor of FGMs and $S_{ijkl}(\boldsymbol{x}) \neq S_{ijkl}(\mathrm{tip})$ for $\boldsymbol{x} \neq \boldsymbol{0}$ as shown in Figure 4. Notice that, in this case, the auxiliary stress fields in Equations (10) and (20) are in equilibrium, i.e. $\sigma_{ij,j}^{aux} = 0$ (no body forces), however, the auxiliary strain field in Equation (22) is not compatible with the auxiliary displacement field, i.e. $\varepsilon_{ij}^{aux} \neq (u_{i,j}^{aux} + u_{j,i}^{aux})/2$. This incompatibility must be considered in the interaction integral formulation. The formulation was first proposed by Dolbow and Gosz (2002) to evaluate SIFs for nonhomogeneous isotropic materials.

Alternative formulations, using the auxiliary fields for homogeneous orthotropic materials (see previous subsections), can also be developed. For instance, one can use compatible displacements and strains, and a constant constitutive tensor around the crack tip. This choice

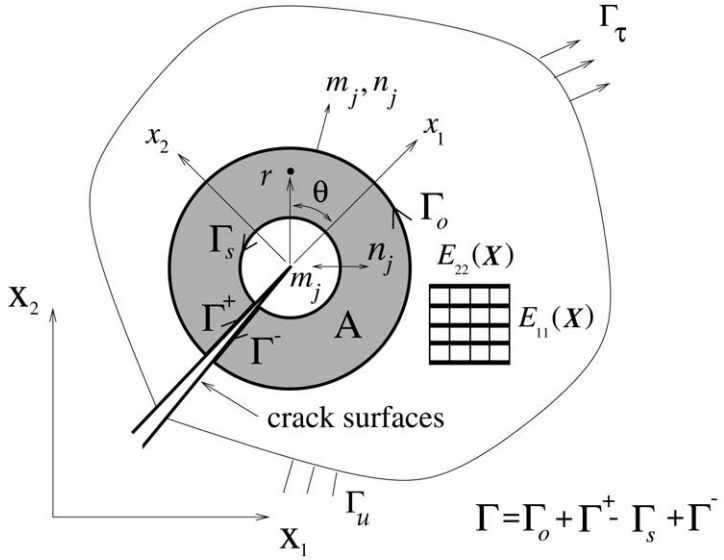

Figure 5. Conversion of the contour integral into an equivalent domain integral (EDI) where $\Gamma = \Gamma_o + \Gamma^+ - \Gamma_s + \Gamma^-$, $m_j = n_j$ on Γ_o and $m_j = -n_j$ on Γ_s.

of auxiliary fields violates the stress-strain relationship in FGMs, while it satisfies compatibility and equilibrium. Another alternative is to use compatible displacements and strains, and the actual constitutive tensor of FGMs. This formulation violates equilibrium, while it satisfies compatibility and the stress-strain relationship. This 'non-equilibrium formulation' was proposed by Paulino and Kim (2004) to evaluate the T-stress in isotropic FGMs.

5. The interaction integral: M-integral

The interaction integral is derived from the path-independent J-integral (Rice, 1968) for two admissible states of a cracked elastic orthotropic FGM. Therefore, the interaction integral (M-integral[1]) is a two-state integral. For the sake of numerical efficiency, the interaction integral employs an equivalent domain integral (EDI) (Raju and Shivakumar, 1990) form. The theoretical formulation, extraction of T-stress, and numerical aspects are provided below.

5.1. M-INTEGRAL: FORMULATION

The standard J-integral (Rice, 1968) is given by

$$J = \lim_{\Gamma_s \to 0} \int_{\Gamma_s} (\mathcal{W}\delta_{1j} - \sigma_{ij}\, u_{i,1})\, n_j\, d\Gamma, \tag{23}$$

where $\mathcal{W}$ is the strain energy density expressed by

$$\mathcal{W} = \frac{1}{2}\sigma_{ij}\varepsilon_{ij} = \frac{1}{2}\, C_{ijkl}\varepsilon_{kl}\varepsilon_{ij}, \tag{24}$$

[1]Here, the so-called M-integral should not be confused with the M-integral (conservation integral) of Knowles and Sternberg (1972), Budiansky and Rice (1973), and Chang and Chien (2002). Also, see the book by Kanninen and Popelar (1985) for a review of conservation integrals in fracture mechanics.

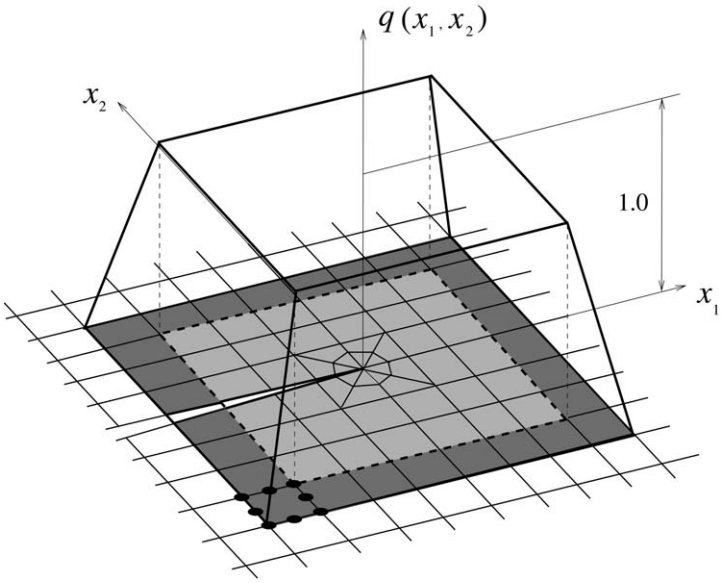

Figure 6. Plateau weight function (q-function).

and n_j is the outward normal vector to the contour Γ_s, as shown in Figure 5. To convert the contour integral into an EDI, the following contour integral is defined:

$$\mathcal{H} = \oint_{\Gamma} (W\delta_{1j} - \sigma_{ij}\, u_{i,1})\, m_j q\, d\Gamma, \tag{25}$$

where Γ=$\Gamma_o + \Gamma^+ - \Gamma_s + \Gamma^-$, m_j is a unit vector outward normal to the corresponding contour (i.e. m_j=n_j on Γ_o and m_j=-n_j on Γ_s), and q is an admissible weight function varying from $q = 1$ on Γ_s to $q = 0$ on Γ_o (see Figure 6). Taking the limit $\Gamma_s \to 0$ leads to

$$\begin{aligned}
\lim_{\Gamma_s\to 0} \mathcal{H} &= \lim_{\Gamma_s\to 0} \oint_{\Gamma} (\mathcal{W}\delta_{1j} - \sigma_{ij}\, u_{i,1})\, m_j q\, d\Gamma \\
&= \lim_{\Gamma_s\to 0} \int_{\Gamma_o+\Gamma^++\Gamma^--\Gamma_s} (\mathcal{W}\delta_{1j} - \sigma_{ij}\, u_{i,1})\, m_j q\, d\Gamma \\
&= \lim_{\Gamma_s\to 0} \left[\int_{\Gamma_o+\Gamma^++\Gamma^-} (\mathcal{W}\delta_{1j} - \sigma_{ij}\, u_{i,1})\, m_j q\, d\Gamma + \int_{-\Gamma_s} (\mathcal{W}\delta_{1j} - \sigma_{ij}\, u_{i,1})\, m_j q\, d\Gamma \right] \\
&= \lim_{\Gamma_s\to 0} \left[\int_{\Gamma_o+\Gamma^++\Gamma^-} (\mathcal{W}\delta_{1j} - \sigma_{ij}\, u_{i,1})\, m_j q\, d\Gamma - \int_{\Gamma_s} (\mathcal{W}\delta_{1j} - \sigma_{ij}\, u_{i,1})\, n_j q\, d\Gamma \right].
\end{aligned} \tag{26}$$

Because $q = 0$ on Γ_o and the crack faces are assumed to be traction-free, one obtains

$$J = -\lim_{\Gamma_s\to 0} \mathcal{H} = -\lim_{\Gamma_s\to 0} \oint_{\Gamma} (\mathcal{W}\delta_{1j} - \sigma_{ij}\, u_{i,1})\, m_j q\, d\Gamma. \tag{27}$$

Applying the divergence theorem to Equation (27) and using the weight function q, one obtains the EDI as

$$J = \int_A (\sigma_{ij}\, u_{i,1} - \mathcal{W}\delta_{1j})\, q_{,j}\, dA + \int_A (\sigma_{ij}\, u_{i,1} - \mathcal{W}\delta_{1j})_{,j}\, q\, dA. \tag{28}$$

The J-integral of the superimposed fields (actual and auxiliary fields) is given as:

$$\begin{aligned} J^s &= \int_A \left\{ (\sigma_{ij} + \sigma_{ij}^{aux})\ (u_{i,1} + u_{i,1}^{aux}) - \frac{1}{2}(\sigma_{ik} + \sigma_{ik}^{aux})(\varepsilon_{ik} + \varepsilon_{ik}^{aux})\delta_{1j} \right\} q_{,j}\ dA \\ &+ \int_A \left\{ (\sigma_{ij} + \sigma_{ij}^{aux})\ (u_{i,1} + u_{i,1}^{aux}) - \frac{1}{2}(\sigma_{ik} + \sigma_{ik}^{aux})(\varepsilon_{ik} + \varepsilon_{ik}^{aux})\delta_{1j}) \right\}_{,j} q\ dA, \end{aligned} \tag{29}$$

which is conveniently decomposed into

$$J^s = J + J^{aux} + M, \tag{30}$$

where J^{aux} is given by

$$J^{aux} = \int_A (\sigma_{ij}^{aux}\ u_{i,1}^{aux} - \mathcal{W}^{aux}\delta_{1j})\ q_{,j}\ dA + \int_A \left\{ \sigma_{ij}^{aux}\ u_{i,1}^{aux} - \frac{1}{2}\sigma_{ik}^{aux}\varepsilon_{ik}^{aux}\delta_{1j} \right\}_{,j} q\ dA, \tag{31}$$

and the resulting general form of the interaction integral (M) is given by

$$\begin{aligned} M &= \int_A \left\{ \sigma_{ij}u_{i,1}^{aux} + \sigma_{ij}^{aux}u_{i,1} - \frac{1}{2}(\sigma_{ik}\varepsilon_{ik}^{aux} + \sigma_{ik}^{aux}\varepsilon_{ik})\delta_{1j} \right\} q_{,j} dA \\ &+ \int_A \left\{ \sigma_{ij}u_{i,1}^{aux} + \sigma_{ij}^{aux}u_{i,1} - \frac{1}{2}(\sigma_{ik}\varepsilon_{ik}^{aux} + \sigma_{ik}^{aux}\varepsilon_{ik})\delta_{1j} \right\}_{,j} q\ dA. \end{aligned} \tag{32}$$

The specific interaction integral (M), based on the incompatibility formulation, is derived as follows. Using the following identity

$$\sigma_{ij}\varepsilon_{ij}^{aux} = \sigma_{ij}C_{ijkl}(\boldsymbol{x})\sigma_{kl}^{aux} = \sigma_{kl}^{aux}\varepsilon_{kl} = \sigma_{ij}^{aux}\varepsilon_{ij}, \tag{33}$$

one rewrites Equation (32) as

$$\begin{aligned} M &= \int_A \left\{ \sigma_{ij}u_{i,1}^{aux} + \sigma_{ij}^{aux}u_{i,1} - \sigma_{ik}\varepsilon_{ik}^{aux}\delta_{1j} \right\} q_{,j} dA \\ &+ \int_A \left\{ \sigma_{ij}u_{i,1}^{aux} + \sigma_{ij}^{aux}u_{i,1} - \sigma_{ik}\varepsilon_{ik}^{aux}\delta_{1j} \right\}_{,j} q\ dA \\ &= M_1 + M_2. \end{aligned} \tag{34}$$

Moreover, the last term of the second integral (M_2) in Equation (34) is expressed as

$$\begin{aligned} (\sigma_{ik}\varepsilon_{ik}^{aux}\delta_{1j})_{,j} &= (\sigma_{ij}\varepsilon_{ij}^{aux})_{,1} = (C_{ijkl}\varepsilon_{kl}\varepsilon_{ij}^{aux})_{,1} \\ &= C_{ijkl,1}\varepsilon_{kl}\varepsilon_{ij}^{aux} + C_{ijkl}\varepsilon_{kl,1}\varepsilon_{ij}^{aux} + C_{ijkl}\varepsilon_{kl}\varepsilon_{ij,1}^{aux} \\ &= C_{ijkl,1}\varepsilon_{kl}\varepsilon_{ij}^{aux} + \sigma_{ij}^{aux}\varepsilon_{ij,1} + \sigma_{ij}\varepsilon_{ij,1}^{aux}. \end{aligned} \tag{35}$$

Substitution of Equation (35) into M_2 in Equation (34) leads to

$$\begin{aligned} M_2 &= \int_A \left(\sigma_{ij,j}u_{i,1}^{aux} + \sigma_{ij}u_{i,1j}^{aux} + \sigma_{ij,j}^{aux}u_{i,1} + \sigma_{ij}^{aux}u_{i,1j}\right) q\ dA \\ &- \int_A \left(C_{ijkl,1}\varepsilon_{kl}\varepsilon_{ij}^{aux} + \sigma_{ij}^{aux}\varepsilon_{ij,1} + \sigma_{ij}\varepsilon_{ij,1}^{aux}\right) q\ dA. \end{aligned} \tag{36}$$

Using equilibrium (actual and auxiliary) and compatibility (actual), one simplifies M_2 in Equation (36) as

$$M_2 = \int_A \left\{\sigma_{ij}(u^{aux}_{i,1j} - \varepsilon^{aux}_{ij,1}) - C_{ijkl,1}\varepsilon_{kl}\varepsilon^{aux}_{ij}\right\} q\ dA.$$

Therefore the resulting interaction integral (M) becomes

$$\begin{aligned} M \ = \ & \int_A \left\{\sigma_{ij}u^{aux}_{i,1} + \sigma^{aux}_{ij}u_{i,1} - \sigma_{ik}\varepsilon^{aux}_{ik}\delta_{1j}\right\} q_{,j}dA \\ & + \int_A \left\{\underline{\sigma_{ij}(u^{aux}_{i,1j} - \varepsilon^{aux}_{ij,1})} - C_{ijkl,1}\varepsilon_{kl}\varepsilon^{aux}_{ij}\right\} q\ dA, \end{aligned} \tag{37}$$

where the underlined term is an incompatible term, which appears due to incompatibility of the auxiliary strain fields. The incompatibility formulation for the extraction of mixed-mode SIFs in isotropic FGMs was first developed by Dolbow and Gosz (2002).

5.2. M-INTEGRAL: THE EXISTENCE OF THE M-INTEGRAL FOR FGMS

The existence of the integral in Equation (37) as r goes to zero is proved below. The term $\sigma_{ij}\varepsilon^{aux}_{ij,1}$ in Equation (37) can be written as

$$\begin{aligned} \sigma_{ij}\varepsilon^{aux}_{ij,1} \ &= \ \sigma_{ij}\{S_{ijkl,1}(\boldsymbol{x})\ \sigma^{aux}_{kl} + S_{ijkl}(\boldsymbol{x})\ \sigma^{aux}_{kl,1}\} \\ &= \ \sigma_{ij}(S_{ijkl})_{\text{tip}}\ \sigma^{aux}_{kl,1} + \sigma_{ij}S_{ijkl,1}(\boldsymbol{x})\ \sigma^{aux}_{kl} + \underline{\sigma_{ij}(S_{ijkl}(\boldsymbol{x}) - (S_{ijkl})_{\text{tip}})\ \sigma^{aux}_{kl,1}} \\ &= \ \sigma_{ij}u^{aux}_{i,1j} + \sigma_{ij}S_{ijkl,1}(\boldsymbol{x})\ \sigma^{aux}_{kl} + \underline{\sigma_{ij}(S_{ijkl}(\boldsymbol{x}) - (S_{ijkl})_{\text{tip}})\ \sigma^{aux}_{kl,1}}. \end{aligned} \tag{38}$$

Thus

$$\sigma_{ij}(u^{aux}_{i,1j} - \varepsilon^{aux}_{ij,1}) = -\sigma_{ij}S_{ijkl,1}(\boldsymbol{x})\ \sigma^{aux}_{kl} - \underline{\sigma_{ij}(S_{ijkl}(\boldsymbol{x}) - (S_{ijkl})_{\text{tip}})\ \sigma^{aux}_{kl,1}}, \tag{39}$$

where the first term of the right hand expression vanishes as r goes to zero because of smoothness assumption of the constitutive tensor, and we focus on the underlined term. The compliance tensor involving material properties must be continuous and differentiable function, and thus it can be written as (Eischen, 1987)

$$S_{ijkl}(r,\theta) = (S_{ijkl})_{tip} + rS^{(1)}_{ijkl}(\theta) + \frac{r^2}{2}S^{(2)}_{ijkl}(\theta) + O(r^3) + \ldots, \tag{40}$$

where $S^{(n)}_{ijkl}(\theta)$ $(n = 1, 2, \ldots)$ are angular functions. For the auxiliary fields for T-stress ($\boldsymbol{u}^{aux} = O(\ln r)$, $\boldsymbol{\sigma}^{aux} = O(r^{-1})$), the integral, as the limit r goes to zero, becomes

$$\begin{aligned} \lim_{A\to 0}\int_A \sigma_{ij}(u^{aux}_{i,1j} - \varepsilon^{aux}_{ij,1})\ q\ dA \ &= \ \lim_{r\to 0}\int_\theta\int_r \sigma_{ij}(u^{aux}_{i,1j} - \varepsilon^{aux}_{ij,1})qrdrd\theta \\ &= \ -\lim_{r\to 0}\int_\theta\int_r \sigma_{ij}(S_{ijkl}(r,\theta) - (S_{ijkl})_{tip})\sigma^{aux}_{kl,1}qrdrd\theta \\ &= \ -\lim_{r\to 0}\int_\theta\int_r O(r^{-1/2})O(r)O(r^{-2})qrdrd\theta \\ &= \ -\lim_{r\to 0}\ O(r^{1/2}) = 0. \end{aligned} \tag{41}$$

The integral involving material derivatives ($C_{ijkl,1}$) in Equation (37) vanishes for the following reason. Derivatives of the elastic moduli are assumed to be bounded at the crack tip, i.e. $C_{ijkl,1}$ is $O(r^\alpha)$ with $\alpha \geq 0$. Therefore, as the limit r goes to zero, the integral becomes

$$\begin{aligned}\lim_{A\to 0}\int_A C_{ijkl,1}\varepsilon_{kl}\varepsilon_{ij}^{aux}q dA &= \lim_{r\to 0}\int_\theta\int_r C_{ijkl,1}\,\varepsilon_{kl}\,\varepsilon_{ij}^{aux}\,q\,r dr d\theta \\ &= \lim_{r\to 0}\int_\theta\int_r O(r^\alpha)O(r^{-1/2})O(r^{-1})\,q\,r\,dr\,d\theta \\ &= \lim_{r\to 0} O(r^{\alpha+1/2}) = 0.\end{aligned} \tag{42}$$

Thus the limit exists and the proposed integral is well-posed.

5.3. M-INTEGRAL: EXTRACTION OF THE T-STRESS

The procedure for extracting the T-stress in orthotropic FGMs is the same as that for isotropic FGMs, which is explained in detail by Kim and Paulino (2003a) and Paulino and Kim (2004). The T-stress can be extracted from the interaction integral taking the limit $r \to 0$ of the domain A shown in Figure 5. By doing so, the contributions of the higher-order (i.e. $O(r^{1/2})$ and higher) and singular (i.e. $O(r^{-1/2})$) terms vanish.

Equation (32) is rewritten as

$$M_{\text{local}} = \int_A \left[\left\{(\sigma_{ij}u_{i,1}^{aux} + \sigma_{ij}^{aux}u_{i,1}) - \frac{1}{2}(\sigma_{ik}\varepsilon_{ik}^{aux} + \sigma_{ik}^{aux}\varepsilon_{ik})\delta_{1j}\right\} q\right]_{,j} dA, \tag{43}$$

where M_{local} denotes the M-integral with respect to local coordinates (x_1, x_2) (see Figure 5). By applying the divergence theorem to Equation (43), one obtains

$$M_{\text{local}} = \lim_{\Gamma_s\to 0}\oint_\Gamma \left\{(\sigma_{ij}u_{i,1}^{aux} + \sigma_{ij}^{aux}u_{i,1}) - \frac{1}{2}(\sigma_{ik}\varepsilon_{ik}^{aux} + \sigma_{ik}^{aux}\varepsilon_{ik})\delta_{1j}\right\} m_j q\, d\Gamma. \tag{44}$$

Because m_j=-n_j and $q = 1$ on Γ_s, m_j=n_j and $q = 0$ on Γ_o, and the crack faces are assumed to be traction-free, then Equation (44) becomes

$$M_{\text{local}} = \lim_{\Gamma_s\to 0}\int_{\Gamma_s}\left[\frac{1}{2}(\sigma_{ik}\varepsilon_{ik}^{aux} + \sigma_{ik}^{aux}\varepsilon_{ik})\delta_{1j} - (\sigma_{ij}u_{i,1}^{aux} + \sigma_{ij}^{aux}u_{i,1})\right] n_j\, d\Gamma. \tag{45}$$

Using the equality in Equation (33), one reduces Equation (45) to

$$M_{\text{local}} = \lim_{\Gamma_s\to 0}\int_{\Gamma_s}\left[\sigma_{ik}\varepsilon_{ik}^{aux}\delta_{1j} - (\sigma_{ij}u_{i,1}^{aux} + \sigma_{ij}^{aux}u_{i,1})\right] n_j\, d\Gamma. \tag{46}$$

The actual stress fields are given by

$$\sigma_{ij} = K_I(2\pi r)^{-1/2} f_{ij}^I(\theta, \mu_1^{\text{tip}}, \mu_2^{\text{tip}}) + K_{II}(2\pi r)^{-1/2} f_{ij}^{II}(\theta, \mu_1^{\text{tip}}, \mu_2^{\text{tip}}) + T\delta_{1i}\delta_{1j} + O(r^{1/2}), \tag{47}$$

where the functions $f_{ij}^I(\theta, \mu_1^{\text{tip}}, \mu_2^{\text{tip}})$ and $f_{ij}^{II}(\theta, \mu_1^{\text{tip}}, \mu_2^{\text{tip}})$ $(i, j = 1,2)$ are given in Equation (7). As the contour Γ_s (see Figure 5) shrinks to the crack tip region, the higher-order terms cancel out as mentioned above. Moreover, there is no contribution from the singular terms $O(r^{-1/2})$ because the integrations from $\theta = -\pi$ to $+\pi$ of angular functions (coefficients) of the three terms given in Equation (46) are cancelled out, and become zero regardless of the resulting singularity $O(r^{-1/2})$.

According to the above argument, the only term that contributes to M is the term involving T. Thus we can consider only the stress parallel to the crack direction:

$$\sigma_{ij} = T\delta_{1i}\delta_{1j}. \tag{48}$$

Substituting Equation (48) into Equation (46), one obtains

$$M_{\text{local}} = -\lim_{\Gamma_s \to 0} \int_{\Gamma_s} \sigma_{ij}^{aux} n_j u_{i,1}\, d\Gamma = T a_{11}^{\text{tip}} \lim_{\Gamma_s \to 0} \int_{\Gamma_s} \sigma_{ij}^{aux} n_j\, d\Gamma. \tag{49}$$

Because the force f is in equilibrium (see Figure 3)

$$f = -\lim_{\Gamma_s \to 0} \int_{\Gamma_s} \sigma_{ij}^{aux} n_j\, d\Gamma, \tag{50}$$

and thus the following simple and important relationship is obtained

$$T = \frac{M_{\text{local}}}{f a_{11}^{\text{tip}}}, \tag{51}$$

where a_{11}^{tip} is a material parameter at the crack tip location based on the local coordinates for plane stress, and is replaced by b_{11}^{tip} for plane strain (cf. Equation (4)). For isotropic materials, Equation (51) becomes

$$T = \frac{E_{\text{tip}}^*}{f} M_{\text{local}}, \tag{52}$$

where $E_{\text{tip}}^* = E_{\text{tip}}$ for plane stress and $E_{\text{tip}}/(1 - \nu_{\text{tip}}^2)$ for plane strain.

6. Finite Element Implementation: I-FRANC2D

The FEM numerical computation for displacements, strains, stresses, etc., is based on the global coordinate system. Therefore the M-integral is first evaluated based on the global coordinate system and then transformed to the local coordinate system. With the coordinate transformation, the M-integral is given by ($i, j = 1, 2$)

$$(M_i)_{\text{local}} = \alpha_{ij}(\theta)(M_j)_{\text{global}}, \quad \alpha_{ij}(\theta) = \begin{bmatrix} \cos\theta & \sin\theta \\ -\sin\theta & \cos\theta \end{bmatrix}. \tag{53}$$

The global quantities $(M_m)_{\text{global}}$ ($m = 1, 2$) are first computed:

$$\begin{aligned} (M_m)_{\text{global}} &= \int_A \left\{ \sigma_{ij} u_{i,m}^{aux} + \sigma_{ij}^{aux} u_{i,m} - \sigma_{ik} \varepsilon_{ik}^{aux} \delta_{mj} \right\} \frac{\partial q}{\partial X_j}\, dA \\ &+ \int_A \left\{ \underline{\sigma_{ij}(u_{i,mj}^{aux} - \varepsilon_{ij,m}^{aux})} - C_{ijkl,m} \varepsilon_{ij} \varepsilon_{kl}^{aux} \right\} q\, dA, \end{aligned} \tag{54}$$

where the term underlined indicates the incompatibility term arising in the formulation. The local quantity M_{local} is evaluated by using the transformation given by Equation (53), i.e.

$$M_{\text{local}} = (M_1)_{\text{local}} = (M_1)_{\text{global}} \cos\theta + (M_2)_{\text{global}} \sin\theta. \tag{55}$$

The FEM code I-FRANC2D (Illinois -FRANC2D) has been used for implementing the interaction integral formulation, and for obtaining all the numerical results for T-stress presented in this paper. The code I-FRANC2D is based on the FRANC2D (FRacture ANalysis Code 2D)(Wawrzynek, 1987; Wawrzynek and Ingraffea, 1991), which was originally developed at

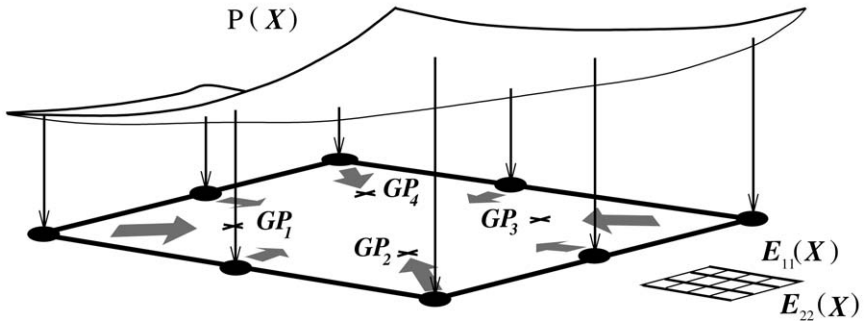

Figure 7. Generalized isoparametric formulation (GIF) (Kim and Paulino, 2002a, 2002b) using graded finite elements. The above figure illustrates a graded Q8 element and $P(\boldsymbol{x})$ denotes a generic material property, e.g. Young's moduli, shear moduli, or Poisson's ratios. The material properties at the Gauss points (P_{GP}) are interpolated from nodal material properties (P_i) by $P_{GP} = \sum N_i P_i$ where $\boldsymbol{N}$ are element shape functions.

Cornell University. The extended capabilities of I-FRANC2D include graded elements to discretize nonhomogeneous isotropic (e.g. *continuum functions* such as exponential, linear, and hyperbolic-tangent material functions; and *micromechanics models* such as self-consistent, Mori-Tanaka, three phase, and differential methods) and orthotropic (e.g. continuum functions) materials. It also includes fracture parameters such as the mixed-mode SIFs and the T-stress.

The graded elements are based on the 'generalized isoparametric formulation' (GIF) (Kim and Paulino, 2002a), which employs an isoparametric finite element and its shape functions (see Figure 7) to discretize geometry, unknowns (displacements), and material properties. In general, graded elements show better performance than conventional homogeneous elements (element-wise constant material property) (Kim and Paulino, 2002b).

Using graded elements, the I-FRANC2D code can evaluate the mixed-mode SIFs and the T-stress for both isotropic and orthotropic FGMs by means of the interaction integral method (Kim and Paulino, 2003a, 2003b). The code can also provide mixed-mode SIFs in FGMs using other numerical schemes such as the path-independent J_k^*-integral, the modified crack closure (MCC), and the displacement correlation technique (DCT) (Kim and Paulino, 2002a, 2002c, 2003c). Based on numerical investigations (Kim and Paulino, 2003a, 2003b; Paulino and Kim, 2004), the interaction integral scheme is observed to be accurate in comparison with the above-mentioned schemes for isotropic and orthotropic FGMs. Therefore, this paper uses this scheme to evaluate the T-stress for cracked orthotropic FGMs.

7. Numerical examples

The performance of the interaction integral method for evaluating the T-stress in orthotropic FGMs is examined by means of several numerical examples. In order to assess the features of the method, the following examples are presented:
(**1**) Inclined center crack in a plate
(**2**) Four-point bending specimen
(**3**) Plate with a single curved crack
(**4**) Plate with two curved cracks
(**5**) Strip with an edge crack

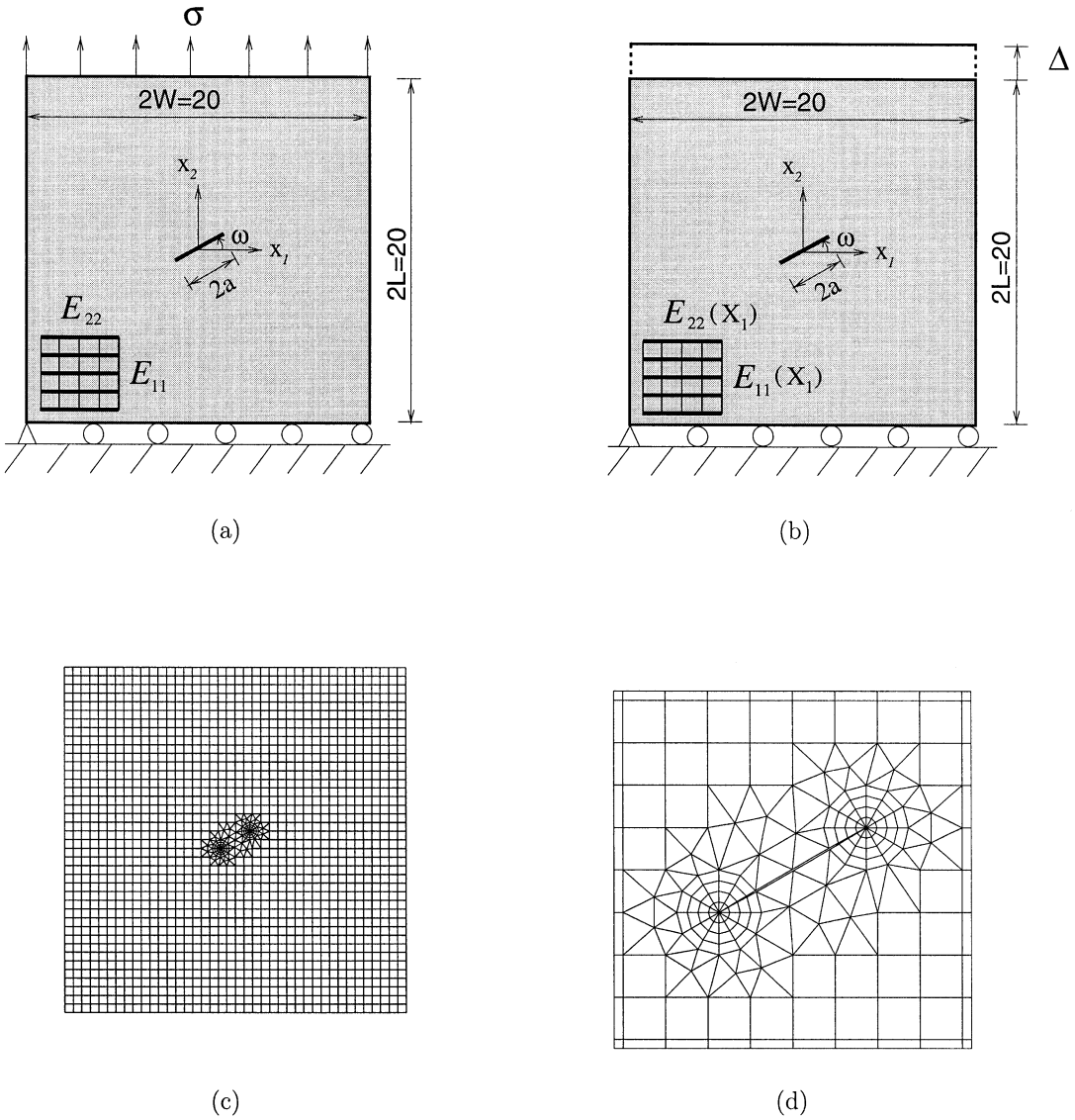

Figure 8. Example 1: plate containing an inclined crack with the angle ω: (a) geometry and BCs for far-field traction; (b) geometry and BCs for fixed-grip loading; (c) complete finite element mesh; (d) mesh detail using 12 sectors (S12) and 4 rings (R4) around the crack tips ($\omega = 30°$ counter-clockwise).

(**6**) Compact tension (CT) specimen

In all the examples, isoparametric graded elements are employed (Kim and Paulino, 2002a). The specific elements used consist of singular quarter-point six-node triangles (T6qp) for crack-tip discretization, eight-node serendipity elements (Q8) for a circular region around crack-tip elements, and regular six-node triangles (T6) in a transition zone to Q8 elements (see, for example, Figure 8).

All the examples consist of T-stress results obtained by means of the interaction integral method in conjunction with the FEM. The first example provides the T-stresses obtained by both the Lehknitskii and Stroh formalisms. The rest of the examples are investigated to

evaluate the T-stress by means of the Lehknitskii formalism. In order to validate T-stress solutions, the first example includes analytical closed-form solutions for an orthotropic homogeneous material, and is investigated for an inclined center crack in a plate ($a/W = 0.1$), which approximates an infinite domain. The same example is investigated for an FGM plate under fixed-grip loading considering exponentially graded material properties. The second example involves a four-point bending specimen with a delamination crack. The third and fourth examples investigate the effect of curved crack(s) in a plate, which naturally involves mode mixity. These two examples allow one to evaluate the effect of crack curvature and multiple cracks on the T-stress. The fifth example investigates an edge crack in a strip considering hyperbolic-tangent material functions, and investigates the effect of translation of the material properties. The last example investigates a compact tension (CT) specimen and provides numerical solutions for the T-stress and the biaxiality ratio considering exponentially graded materials.

7.1. Inclined center crack in a plate

Figures 8a and 8b show an inclined center crack of length $2a$ located with a geometric angle ω (counter-clockwise) in a plate under far-field constant traction and fixed-grip loading, respectively. Figure 8c shows the complete mesh configuration, and Figure 8d shows the mesh detail using crack-tip templates of 12 sectors (S12) and 4 rings (R4) of elements. The displacement boundary condition is prescribed such that $u_2 = 0$ along the lower edge, and $u_1 = 0$ for the node at the lower left hand side. The mesh discretization consists of 1641 Q8, 94 T6, and 24 T6qp elements, with a total of 1759 elements and 5336 nodes. The following data are used for the FEM analysis:

$$\begin{aligned} &\text{plane stress, } 2 \times 2 \text{ Gauss quadrature,} \\ &a/W = 0.1,\ L/W = 1.0,\ \omega = (0^\circ, 15^\circ, 30^\circ, 45^\circ, 60^\circ, 75^\circ, 90^\circ). \end{aligned} \tag{56}$$

7.1.1. *Far-field traction - homogeneous orthotropic plate*

This example is illustrated by Figure 8a, and its discretization is shown in Figures 8c and 8d. For a crack inclined by $\omega = 0^\circ$ (see Figure 8a), where the global Cartesian coordinates coincide with the material orthotropy directions, there is an analytical solution available for the T-stress (e.g. Gao and Chiu, 1992), which is given by

$$T = \sigma_{11}^{\infty} - \sigma_{22}^{\infty}\sqrt{a_{22}/a_{11}}. \tag{57}$$

The applied load corresponds to $\sigma_{22}(X_1, 10) = \sigma$. Young's moduli, shear modulus, and Poisson's ratio are given by

$$E_{11} = 10^4, \quad E_{22} = 10^3, G_{12} = 1216, \quad \nu_{12} = 0.3, \tag{58}$$

respectively.

Table 1 shows the FEM results for the T-stress using the interaction integral in conjunction with either Lekhnitskii or Stroh formalism for various crack angles ω. It shows good agreement between the two FEM results for T-stress for the angle $\omega = 0^\circ$ obtained by the interaction integral method, using the two formalisms, and the closed-form solution given by Equation (57). The two formulations provide similar T-stress results. For a homogeneous material, the T-stress for the right crack-tip is the same as that for the left crack-tip, and this

Table 1. Example 1: T-stress for an inclined center crack in a homogeneous orthotropic plate under *far-field constant traction* – see Figure 8a (angle ω: counter-clockwise).

ω	T		
	Lekhnitskii	Stroh	Exact
0°	−3.164	−3.156	−3.162
15°	−1.643	−1.647	–
30°	0.031	0.030	–
45°	0.716	0.718	–
60°	0.936	0.935	–
75°	0.988	0.988	–
90°	0.996	0.997	1.000

feature is verified by the present FEM implementation. The T-stress increases as the angle ω increases and it changes sign when $\omega \approx 29.5°$. Notice that, as expected, the numerical T-stress for the angle 90° is close to 1.0.

7.1.2. *Fixed-grip loading – nonhomogeneous orthotropic plate*
This example consists of an inclined center crack in an FGM plate subjected to fixed-grip loading. The applied load corresponds to $\sigma_{22}(X_1, 10) = \bar{\varepsilon} E^0_{22} e^{\beta X_1}$ (see Figure 8b). This loading results in a uniform strain $\varepsilon_{22}(X_1, X_2) = \bar{\varepsilon}$ in a corresponding uncracked structure. Young's moduli and shear modulus are exponential functions of X_1, while Poisson's ratio is constant. The material properties are given by

$$E_{11}(X_1) = E^0_{11} e^{\beta X_1},\ E_{22}(X_1) = E^0_{22} e^{\beta X_1}, G_{12}(X_1) = G^0_{12} e^{\beta X_1}, \nu_{12}(X_1) = \nu^0_{12} \tag{59}$$

with

$$E^0_{11} = 10^4,\ E^0_{22} = 10^3, G^0_{12} = 1216,\ \nu^0_{12} = 0.3. \tag{60}$$

The following data are used for the FEM analysis: $\beta a = (0.0, 0.5)$; $\bar{\varepsilon} = 0.001$. Notice that βa is the dimensionless material nonhomogeneity parameter.

Table 2 shows the FEM results for the T-stress using the interaction integral in conjunction with either Lekhnitskii or Stroh formalism for various material parameters βa. The two formulations provide similar results for both homogeneous and FGM cases. For the homogeneous material case ($\beta a = 0.0$), the T-stress increases as the angle ω increases and it changes sign at $\omega \approx 29.5°$. For the FGM case ($\beta a = 0.5$), the T-stress changes sign when $\omega \approx 27.5°$ for the right crack tip and $\omega \approx 28.5°$ for the left crack tip. Moreover, as βa increases, the T-stress for the right crack-tip $T(+a)$ increases within the range $0° \leq \omega \leq 75°$ and remains approximately the same for $\omega = 90°$ (cf. second and fourth columns, and third and fifth columns of Table 2). Also, as βa increases, the T-stress for the left crack-tip $T(-a)$ increases for the range of $0° \leq \omega \leq 30°$, and then decreases for the range of $30° < \omega < 90°$ (cf. second and sixth columns, and third and seventh columns of Table 2).

For the homogeneous material case ($\beta a = 0.0$), the fixed-grip loading (see Figure 8a) is equivalent to the far-field constant traction (see Figure 8b) when considering an infinite

Table 2. Example 1: T-stress for an inclined center crack in an orthotropic plate under *fixed-grip loading* – see Figure 8b (angle ω: counter-clockwise).

ω	$\beta a = 0.0$		$\beta a = 0.5$			
	$T(\pm a)$		$T(+a)$		$T(-a)$	
	Lekhnitskii	Stroh	Lekhnitskii	Stroh	Lekhnitskii	Stroh
0°	−3.129	−3.126	−2.829	−2.832	−2.718	−2.712
15°	−1.630	−1.632	−1.386	−1.384	−1.405	−1.407
30°	0.031	0.030	0.172	0.168	0.075	0.074
45°	0.712	0.714	0.783	0.785	0.700	0.702
60°	0.933	0.932	0.973	0.970	0.911	0.910
75°	0.987	0.987	1.002	1.002	0.973	0.973
90°	0.996	0.997	0.996	0.997	0.996	0.997

domain (i.e. $\bar{\varepsilon} = \sigma/E_{22} = 0.001$) – cf. second and third columns of Table 1 with second and third columns of Table 2, respectively. However, we observe small differences in T-stresses as shown in Tables 1 and 2. The differences may be due to the effect of a finite plate size ($a/W = 0.1$) approximating an infinite domain, and the loading boundary condition (applied traction versus fixed grip) over a finite domain.

7.2. Four-point bending specimen

Gu and Asaro (1997) investigated the effect of material orthotropy on mixed-mode SIFs in FGMs considering a four-point bending specimen with exponentially varying Young's moduli, shear modulus, and Poisson's ratio. Kim and Paulino (2003b) evaluated the SIFs by means of the interaction integral method, and the SIFs agree well with those by Gu and Asaro (1997). Here we focus on the effect of material orthotropy on the T-stress. Figure 9a shows the four-point bending specimen geometry and BCs, Figure 9b shows the complete FEM mesh configuration, Figure 9c shows the mesh detail using 12 sectors (S12) and 4 rings (R4) around the crack tips, and Figure 9d shows an enlarged view of the right crack-tip template. Point loads of magnitude P are applied at the nodes $(X_1, X_2) = (\pm 11, 1.0)$. The displacement boundary conditions are prescribed such that $(u_1, u_2) = (0, 0)$ for the node at $(X_1, X_2) = (-10, -1.0)$ and $u_2 = 0$ for the node at $(X_1, X_2) = (10, -1.0)$. Young's moduli and shear modulus are exponential functions of X_2, while Poisson's ratio is constant. The material properties are given by

$$\begin{aligned} &E_{11}(X_2) = E_{11}^0 e^{\beta X_2},\ E_{22}(X_2) = E_{22}^0 e^{\beta X_2}, G_{12}(X_2) = G_{12}^0 e^{\beta X_2} \\ &\nu_{12}(X_2) = \nu_{12}^0,\ \lambda = E_{22}(X_2)/E_{11}(X_2), \end{aligned} \tag{61}$$

where λ denotes the orthotropy ratio. Moreover, the following numerical values of properties are adopted:

$$\begin{aligned} &\text{For } \lambda = 0.1,\ E_{11}^0 = 1,\ E_{22}^0 = 0.1,\ G_{12}^0 = 0.5,\ \ \nu_{12}^0 = 0.3, \\ &\text{For } \lambda = 1.0,\ E_{11}^0 = 1,\ E_{22}^0 = 1,\ G_{12}^0 = 0.3846,\ \ \nu_{12}^0 = 0.3, \\ &\text{For } \lambda = 10,\ E_{11}^0 = 1,\ E_{22}^0 = 10,\ G_{12}^0 = 0.5,\ \ \nu_{12}^0 = 0.03. \end{aligned} \tag{62}$$

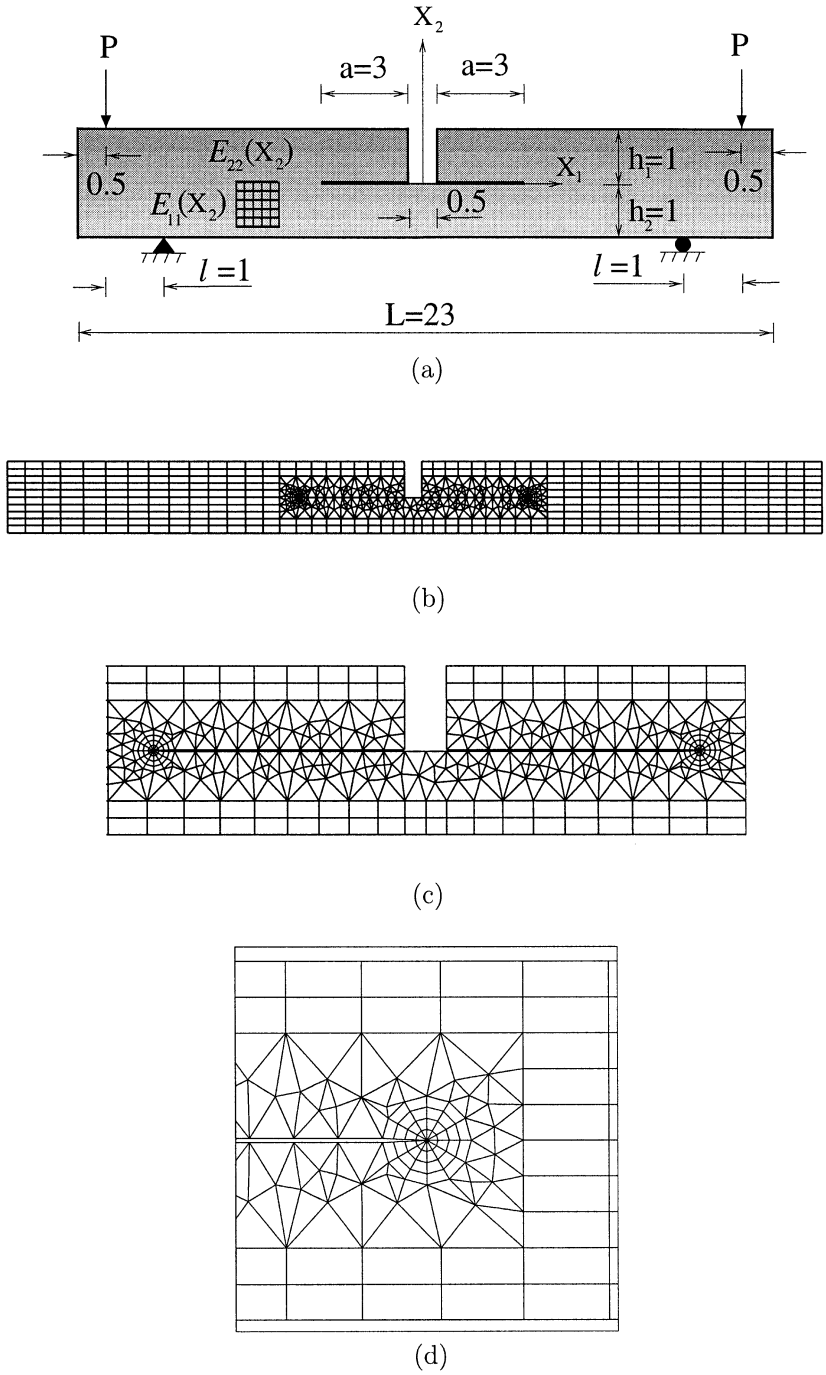

Figure 9. Example 2: Four-point bending specimen: (a) geometry and BCs; (b) complete finite element mesh; (c) mesh detail using 12 sectors (S12) and 4 rings (R4) around crack tips; (d) enlarged view of the right crack tip.

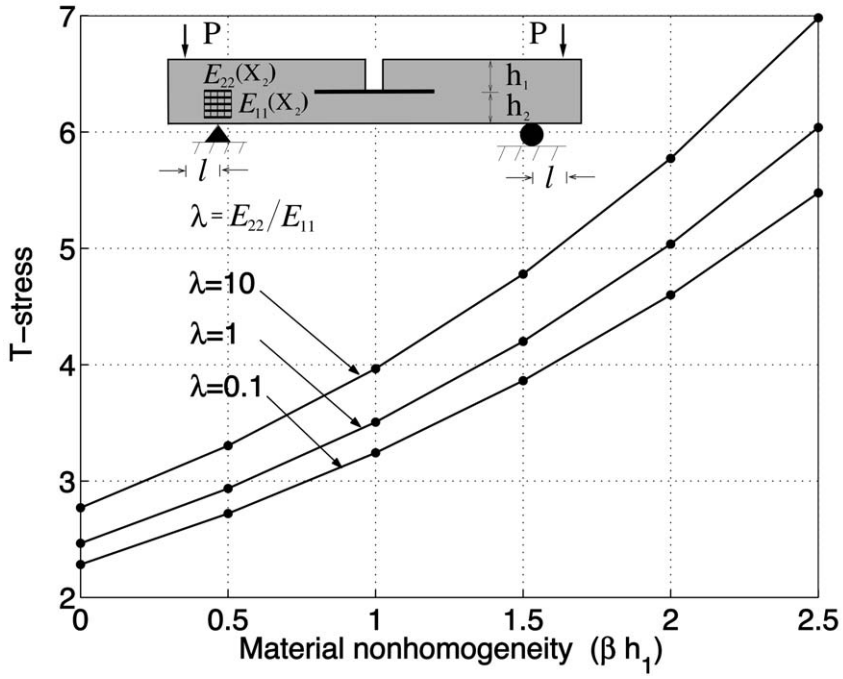

Figure 10. Example 2: T-stress for a four-point bending specimen. The parameter $\lambda = E_{22}/E_{11}$ is the orthotropy ratio. Notice that the parameters λ and βh_1 influence T-stress.

The mesh discretization consists of 625 Q8, 203 T6, and 24 T6qp elements, with a total of 852 elements and 2319 nodes. The following data are used for the FEM analysis:

$$\begin{aligned} &\text{plane stress, } 2 \times 2 \text{ Gauss quadrature,} \\ &\quad a = 3.0,\ h_1/h_2 = 1.0,\ P = 1.0. \end{aligned} \tag{63}$$

Figure 10 shows the FEM results for the T-stress obtained by the interaction integral method in conjunction with the Lekhnitskii formalism. Notice that T-stresses are all positive for the range of the material orthotropy $\lambda = E_{22}/E_{11}$ and material nonhomogeneity parameter βh_1 investigated. The T-stress for the right crack tip is the same that for the left crack tip due to the symmetry, and this feature is captured by the present FEM implementation. There is a significant influence of the material orthotropy λ and material nonhomogeneity βh_1 on the T-stress. As either βh_1 or λ increases, the T-stress increases. With increasing material nonhomogeneity βh_1, the effect of material orthotropy λ on T-stress becomes more pronounced.

7.3. Plate with a single curved crack

Figures 11a and 11b show a single curved crack located in a plate under remote uniform tension loading for two different boundary conditions. These boundary conditions are prescribed such that, for the first set of BCs (Figure 11a), $u_1 = u_2 = 0$ for the node in the middle of the left edge, and $u_2 = 0$ for the node in the middle of the right edge; while for the second set of BCs (Figure 11b), $u_1 = 0$ for the node in the middle of the top edge, and $u_1 = u_2 = 0$ for the node in the middle of the bottom edge. Figure 11c shows the complete finite element mesh configuration, and Figure 11d shows a mesh detail using 12 sectors (S12) and 5 rings (R5)

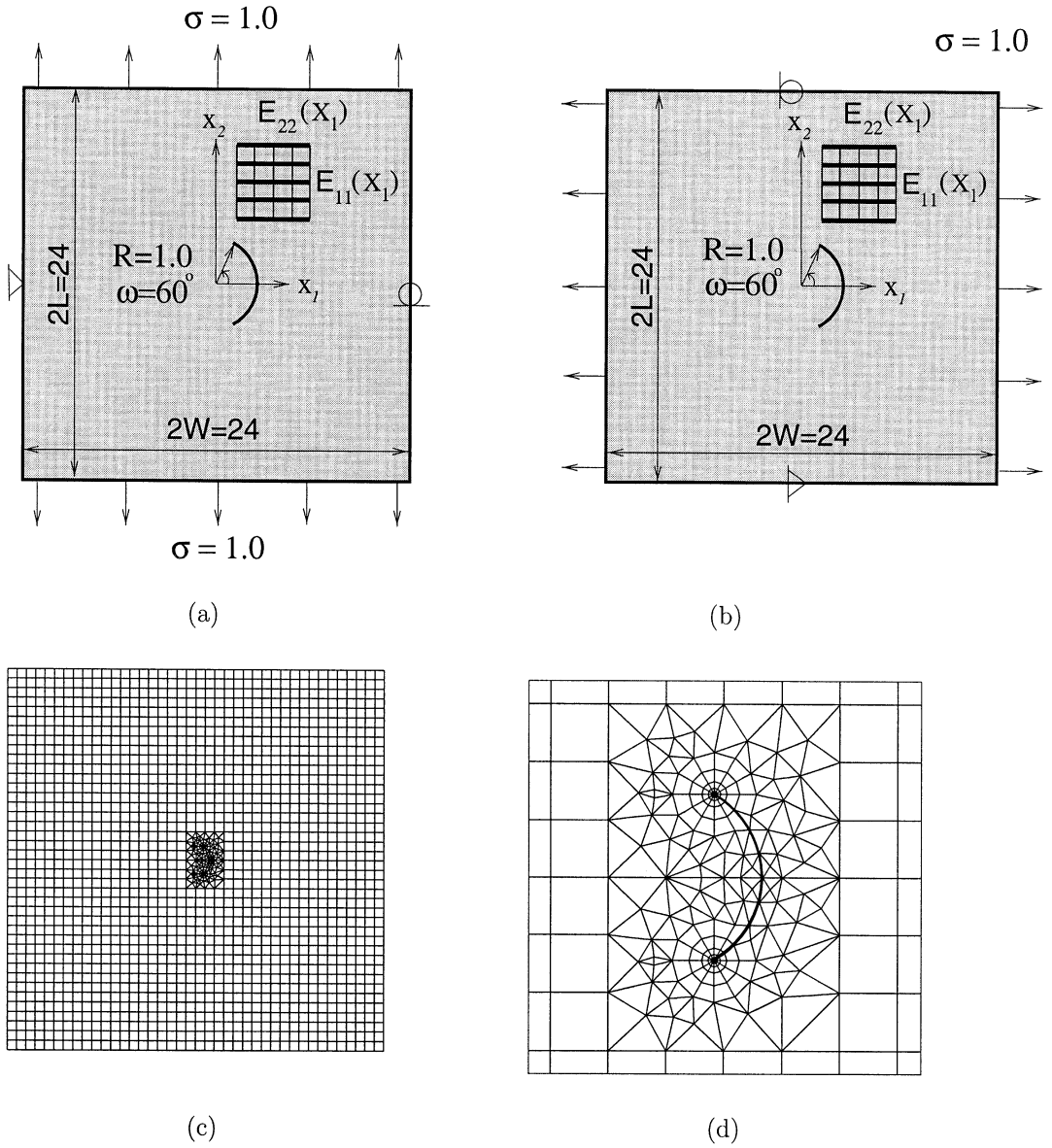

Figure 11. Example 3: plate with a single curved crack: (a) geometry and BCs (first set of BCs); (b) geometry and BCs (second set of BCs); (c) complete finite element mesh; (d) mesh detail with 12 sectors (S12) and 5 rings (R5) around the crack tip (S12,R5) - the thick line indicates the crack faces.

around the crack tips. The applied load corresponds to $\sigma_{22}(X_1, \pm L) = \sigma = 1.0$ for the BC in Figure 11a and $\sigma_{11}(\pm W, X_2) = \sigma = 1.0$ for the BC in Figure 11b. The mesh discretization consists of 1691 Q8, 184 T6, and 24 T6qp elements, with a total of 1875 elements and 5608 nodes. The following data are used in the FEM analyses:

Table 3. Example 3: T-stress for a single curved crack. **Case 1**: first set of BCs – see Figure 11a.

Case	Material	βR	T-stress
	Iso	0.0	−0.3684
1		0.0	−0.2748
		0.1	−0.2724
	Ortho	0.2	−0.2520
		0.3	−0.2099
		0.4	−0.1513
		0.5	−0.0981

Table 4. Example 3: T-stress for a single curved crack. **Case 2**: second set of BCs – see Figure 11b.

Case	Material	βR	T-stress
	Iso	0.0	0.6076
2		0.0	0.4057
		0.1	0.3230
	Ortho	0.2	0.2389
		0.3	0.1516
		0.4	0.0655
		0.5	−0.0185

plane stress, 2×2 Gauss quadrature,

$$R = 1.0, \quad L/W = 1.0,$$

Isotropic case (Homogeneous) :

$$E = 1.0, \ \nu = 0.3$$

Orthotropic case :

$$E_{11}(X_1) = E_{11}^0 e^{\beta X_1}, E_{22}(X_1) = E_{22}^0 e^{\beta X_1}, G_{12}(X_1) = G_{12}^0 e^{\beta X_1}, \nu_{12}(X_1) = \nu_{12}^0,$$

$$E_{11}^0 = 1.0, \ E_{22}^0 = 0.5, \ G_{12}^0 = 0.25, \ \nu_{12}^0 = 0.3,$$

dimensionless nonhomogeneity parameter: $\beta R = (0.0 \text{ to } 0.5)$.

Tables 3 and 4 show FEM results for the T-stress obtained by means of the interaction integral in conjunction with the Lekhnitskii formalism for a single curved crack considering the two sets of boundary conditions illustrated by Figures 11a and 11b and gradation along the X_1 direction. There is a significant influence of material orthotropy and material nonhomogeneity (parameter βR) on the T-stress. Because of symmetry, the T-stress on the top and bottom crack tips are identical. The T-stress for orthotropic homogeneous material differs significantly from that for isotropic homogeneous material. For orthotropic materials, the nonhomogeneity parameter βR increases the T-stress for the first set of BCs (Case 1: Figure 11a, Table 3) and

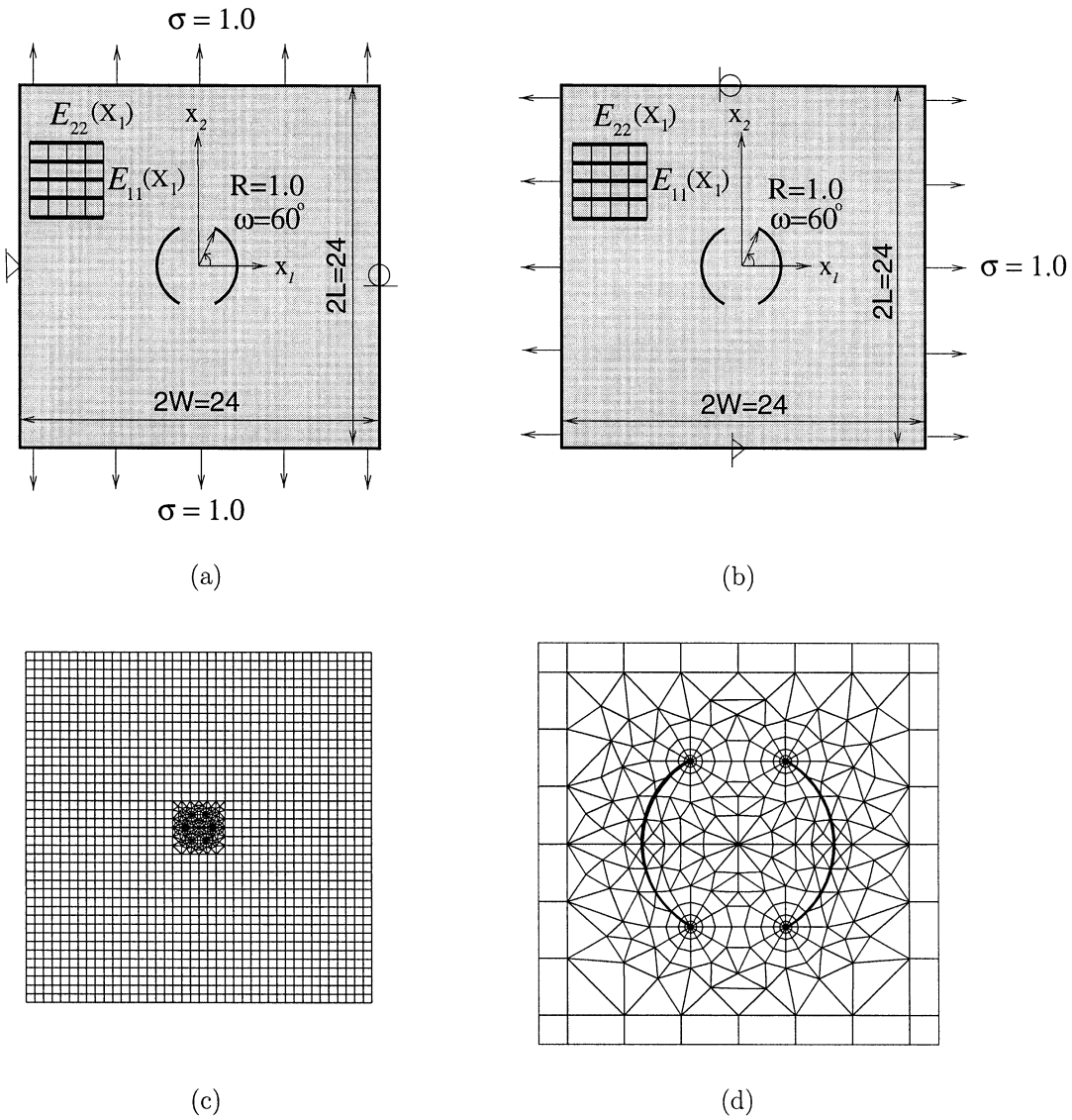

Figure 12. Example 4: plate with two interacting curved cracks: (a) geometry and BCs (first set of BCs); (b) geometry and BCs (second set of BCs); (c) complete finite element mesh; (d) mesh detail with 12 sectors (S12) and 5 rings (R5) around the crack tip (S12,R5) – the thick lines indicate the crack faces.

decreases the T-stress for the second set of BCs (Case 2: Figure 11b, Table 4). Moreover, for Case 1, the T-stress remains negative for the range of βR investigated ($0 \leq \beta R \leq 0.5$), however, for Case 2, it changes sign at $\beta R \approx 0.47$. The change in sign of the T-stress indicates that the nonhomogeneity parameter βR may also influence crack path stability.

7.4. Plate with two curved cracks

Figures 12a and 12b show two curved cracks located in a plate under remote uniform tension loading for two different boundary conditions. These boundary conditions are prescribed such that, for the first set of BCs (Figure 12a), $u_1 = u_2 = 0$ for the node in the middle of the left

Table 5. Example 4: T-stress for two interacting semi-circular cracks. **Case 1**: first set of BCs – Figure 12a.

Case	Material	βR	T (right)	T (left)
	Iso	0.0	−0.3283	−0.3283
1		0.0	−0.2286	−0.2286
		0.1	−0.1854	−0.1828
	Ortho	0.2	−0.0762	−0.0597
		0.3	0.0569	0.0985
		0.4	0.1757	0.2454
		0.5	0.2581	0.3555

edge, and $u_2 = 0$ for the node in the middle of the right edge; while for the second set of BCs (Figure 12b), $u_1 = 0$ for the node in the middle of the top edge and $u_1 = u_2 = 0$ for the node in the middle of the bottom edge. Figure 12c shows the complete finite element mesh configuration, and Figure 12d shows a mesh detail using 12 sectors (S12) and 5 rings (R5) around the crack tips. The applied load corresponds to $\sigma_{22}(X_1, \pm L) = \sigma = 1.0$ for the BC in Figure 12a, and $\sigma_{11}(\pm W, X_2) = \sigma = 1.0$ for the BC in Figure 12b. The mesh discretization consists of 1766 Q8, 260 T6, and 48 T6qp elements, with a total of 2074 elements and 6119 nodes. The following data are used in the FEM analyses:

plane stress, 2×2 Gauss quadrature,

$$R = 1.0, \quad L/W = 1.0,$$

Isotropic case (Homogeneous) :

$$E = 1.0, \ \nu = 0.3$$

Orthotropic case :

$$E_{11}(X_1) = E_{11}^0 e^{\beta X_1}, \ E_{22}(X_1) = E_{22}^0 e^{\beta X_1}, \ G_{12}(X_1) = G_{12}^0 e^{\beta X_1}, \ \nu_{12}(X_1) = \nu_{12}^0$$

$$E_{11}^0 = 1.0, \ E_{22}^0 = 0.5, \ G_{12}^0 = 0.25, \ \nu_{12}^0 = 0.3,$$

dimensionless nonhomogeneity parameter: $\beta R = (0.0 \text{ to } 0.5)$.

Tables 5 and 6 show FEM results for the T-stress obtained by means of the interaction integral in conjunction with the Lekhnitskii formalism for two curved cracks considering the two sets of boundary conditions illustrated by Figures 12a and 12b and gradation along the X_1 direction. There is a significant influence of the material orthotropy and nonhomogeneity parameter βR on the T-stress. Because of symmetry, the T-stresses for all four crack tips are identical for a homogeneous material (βR=0.0) for both cases. For the FGM case, the T-stresses are the same for the top and bottom crack tips. The T-stress for the orthotropic homogeneous material differs significantly from that for the isotropic homogeneous material (cf. first and second rows in Tables 5 and 6). For orthotropic materials, the nonhomogeneity parameter βR increases the T-stress at the right and left crack tips for the Case 1 (see Table 5). However, as βR increases the T-stress decreases at the right crack tip, but increases at the left crack tip for the Case 2 (see Table 6). Moreover, for Case 1, the T-stress changes sign at $\beta R \approx 0.25$, however, for Case 2, the T-stress is positive for the range of βR investigated.

Table 6. Example 4: T-stress for two semi-circular cracks. **Case 2**: second set of BCs – Figure 12b.

Case	Material βR	T (right)		T (left)
	Iso	0.0	0.8353	0.8353
2		0.0	0.6734	0.6734
		0.1	0.6126	0.7269
	Ortho	0.2	0.5478	0.7747
		0.3	0.4845	0.8218
		0.4	0.4269	0.8740
		0.5	0.3775	0.9341

Finally, by comparing the previous example (single curved crack) with the present one (two curved cracks), one notices that the crack interaction effect increases the T-stress.

7.5. Strip with an edge crack

Figure 13a shows an edge crack of length a in an FGM plate, and Figure 13b shows a detail of the mesh discretization using a crack-tip template of 12 sectors (S12) and 4 rings (R4) of elements. Figures 13c, 13d, and 13e illustrate the three considered types of hyperbolic-tangent material gradation with respect to the crack tip: reference configuration, translation to the left, and translation to the right, respectively. The fixed-grip displacement loading results in a uniform strain $\varepsilon_{22}(X_1, X_2) = \bar{\varepsilon}$ in a corresponding uncracked structure. The displacement boundary condition is prescribed such that $u_2 = 0$ along the lower edge and $u_1 = 0$ for the node at the lower left hand side.

Young's moduli and shear modulus are hyperbolic-tangent functions with respect to the global (X_1, X_2) Cartesian coordinates as follows:

$$\begin{aligned} E_{11}(X_1) &= \frac{E_{11}^- + E_{11}^+}{2} + \frac{E_{11}^- - E_{11}^+}{2} \tanh(\alpha(X_1 + d)), \\ E_{22}(X_1) &= \frac{E_{22}^- + E_{22}^+}{2} + \frac{E_{22}^- - E_{22}^+}{2} \tanh(\beta(X_1 + d)), \\ G_{12}(X_1) &= \frac{G_{12}^- + G_{12}^+}{2} + \frac{G_{12}^- - G_{12}^+}{2} \tanh(\gamma(X_1 + d)), \end{aligned} \tag{64}$$

where d is a constant for translation. In this example, the Poisson's ratio ν_{12} is taken as constant. The mesh discretization consists of 784 Q8, 290 T6, and 12 T6qp elements, with a total of 1086 elements and 3107 nodes. The following data are used for the FEM analysis:

$$\text{plane stress, } 2 \times 2 \text{ Gauss quadrature,}$$

$$a/W = 0.5, L/W = 2.0, \bar{\varepsilon} = 0.25,$$

$$d = (-0.5 \text{ to } 0.5), \ \nu_{12} = 0.3,$$

Case 1: Proportional material variation (see Figure 14)

$$\alpha a = \beta a = \gamma a = 15.0,$$

$$(E_{11}^-, E_{11}^+) = (1.00, 3.00), (E_{22}^-, E_{22}^+) = (1.25, 2.75), \ (G_{12}^-, G_{12}^+) = (1.50, 2.50),$$

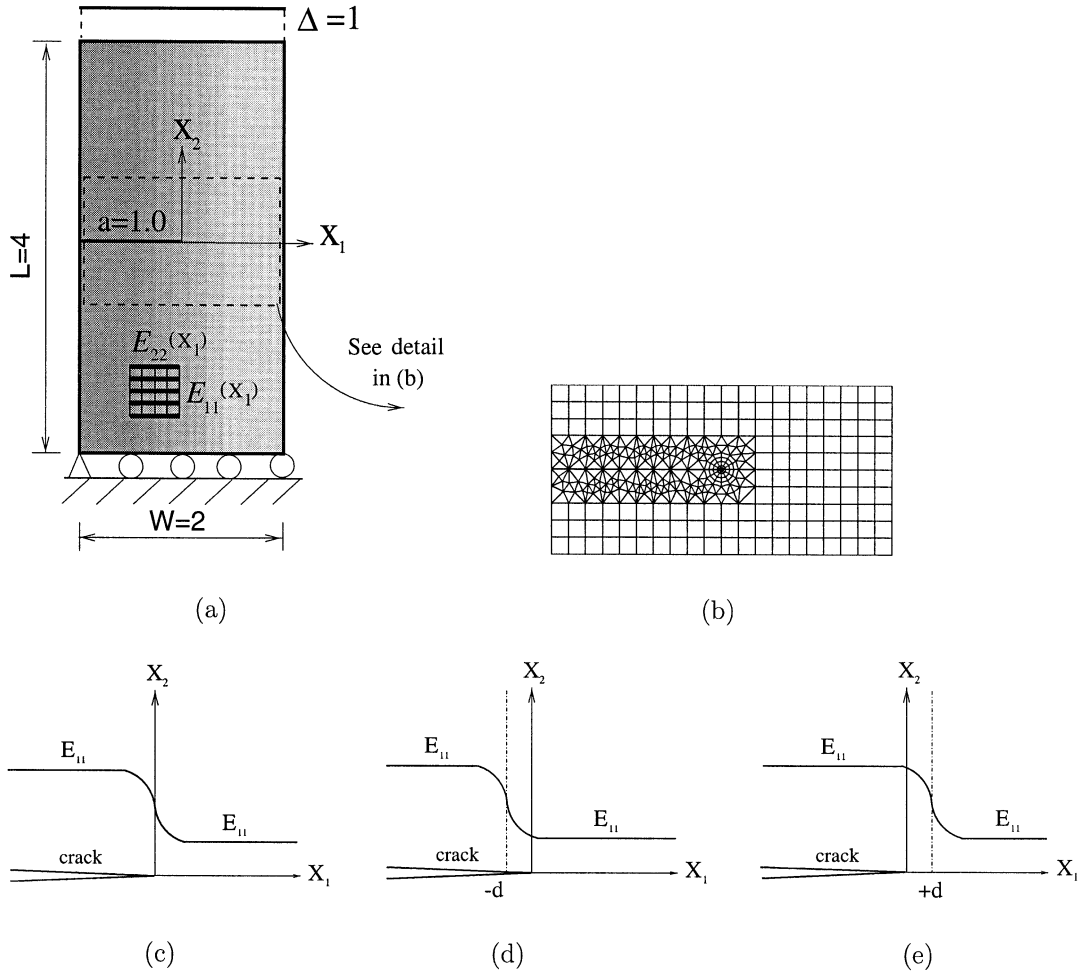

Figure 13. Example 5: Strip with an edge crack in hyperbolic-tangent materials: (a) geometry and BCs; (b) detail of finite element mesh with 12 sectors (S12) and 4 rings (R4) around the crack tip; (c) reference configuration ($d = 0.0$); (d) translation of material gradation to the left ($d = +0.5$); (e) translation of material gradation to the right ($d = -0.5$).

Case 2: Proportional material variation (see Figure 15)

$$\alpha a = \beta a = \gamma a = 15.0,$$

$$(E_{11}^-, E_{11}^+) = (1.00, 5.00), (E_{22}^-, E_{22}^+) = (1.25, 2.75), \ (G_{12}^-, G_{12}^+) = (1.50, 2.50),$$

Case 3: Non-proportional material variation (see Figure 16)

$$\alpha a = 4.0, \beta a = 2.0, \gamma a = 1.0,$$

$$(E_{11}^-, E_{11}^+) = (E_{22}^-, E_{22}^+) = (G_{12}^-, G_{12}^+) = (1.00, 3.00).$$

Table 7 shows the FEM results for the T-stress using the interaction integral in conjunction with the Lekhnitskii formalism for various translation factors of hyperbolic-tangent material variation considering three particular cases of material variations. The negative T-stresses are observed for all the three cases. For proportional material variations (Case 1 and Case 2), the

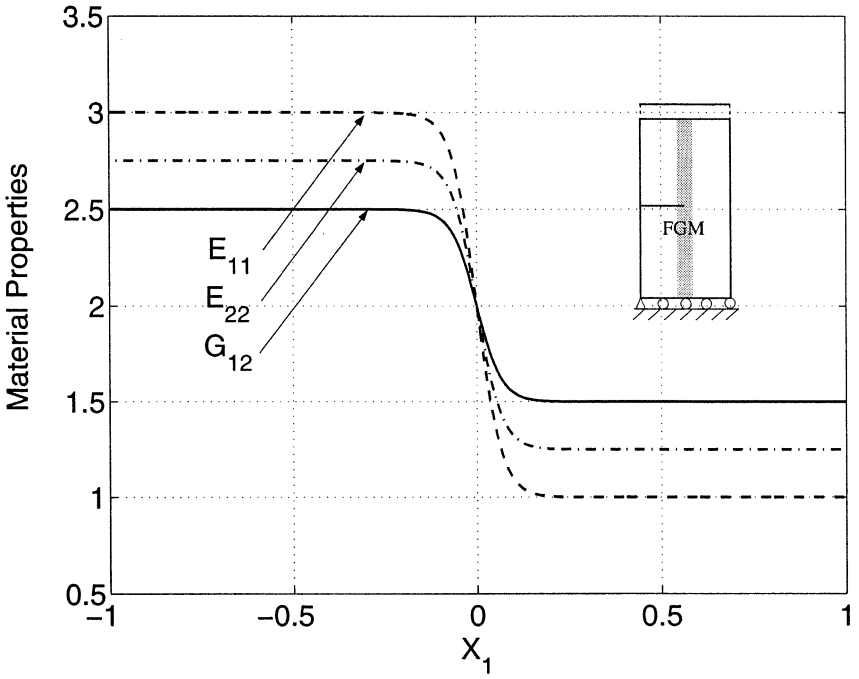

Figure 14. Example 5: *Proportional* variation of material properties (Case 1).

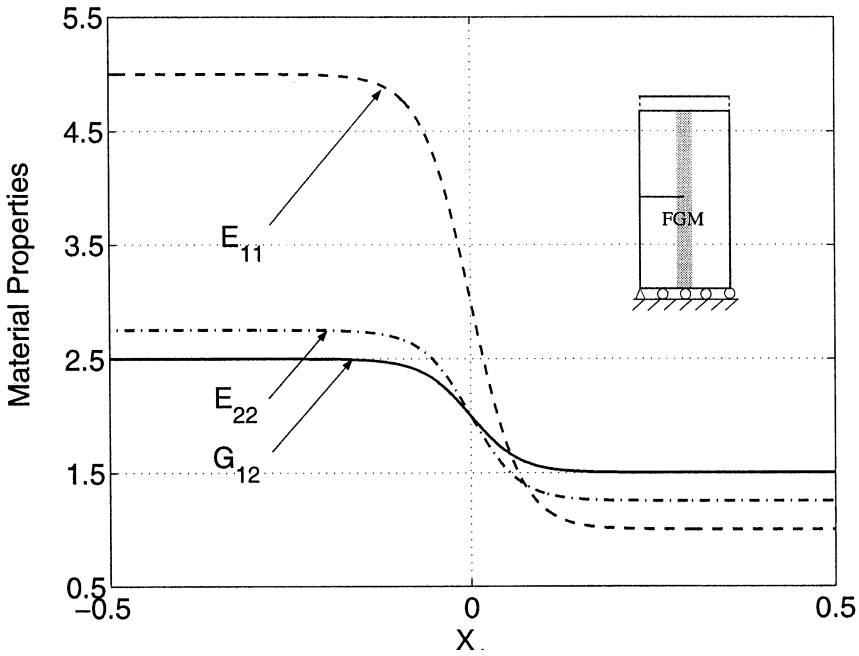

Figure 15. Example 5: *Proportional* variation of material properties (Case 2).

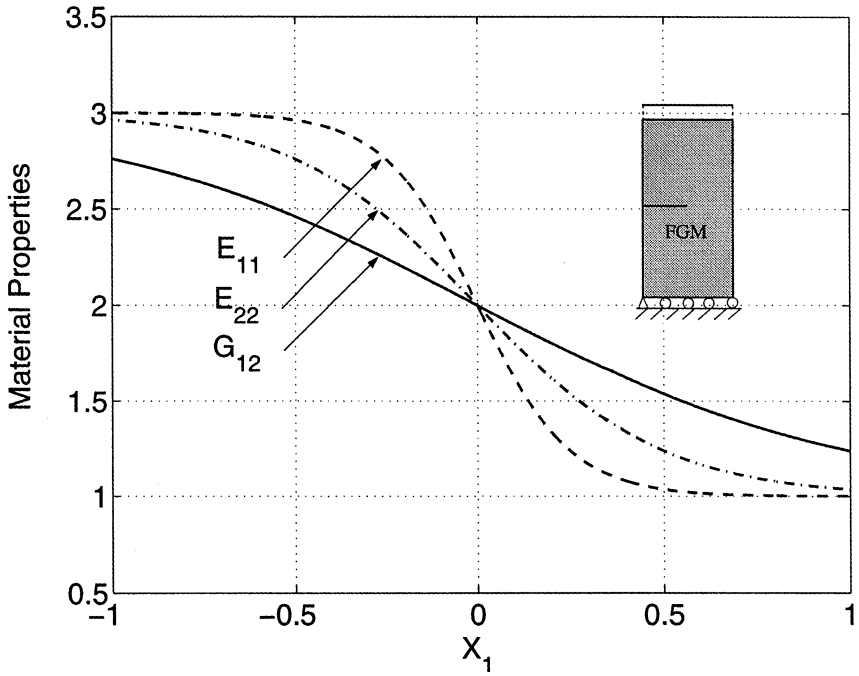

Figure 16. Example 5: *Nonproportional* variation of material properties (Case 3).

Table 7. Example 5: FEM results for the T-stress for an edge crack with translation of hyperbolic-tangent material variation. **Case 1**: proportional material variation (Figure 14); **Case 2**: proportional material variation (Figure 15); **Case 3**: Nonproportional material variation (Figure 16).

d	T		
	Case 1	Case 2	Case 3
−0.5	−0.3886	−0.4982	−0.4373
−0.4	−0.4046	−0.5210	−0.4533
−0.3	−0.4310	−0.5715	−0.4754
−0.2	−0.4999	−0.6928	−0.4929
−0.1	−0.7011	−0.9900	−0.4991
0	−0.9667	−1.3870	−0.4714
0.1	−0.3643	−0.4615	−0.4099
0.2	−0.2051	−0.2248	−0.3369
0.3	−0.1706	−0.1773	−0.2749
0.4	−0.1573	−0.1600	−0.2304
0.5	−0.1516	−0.1527	−0.2001

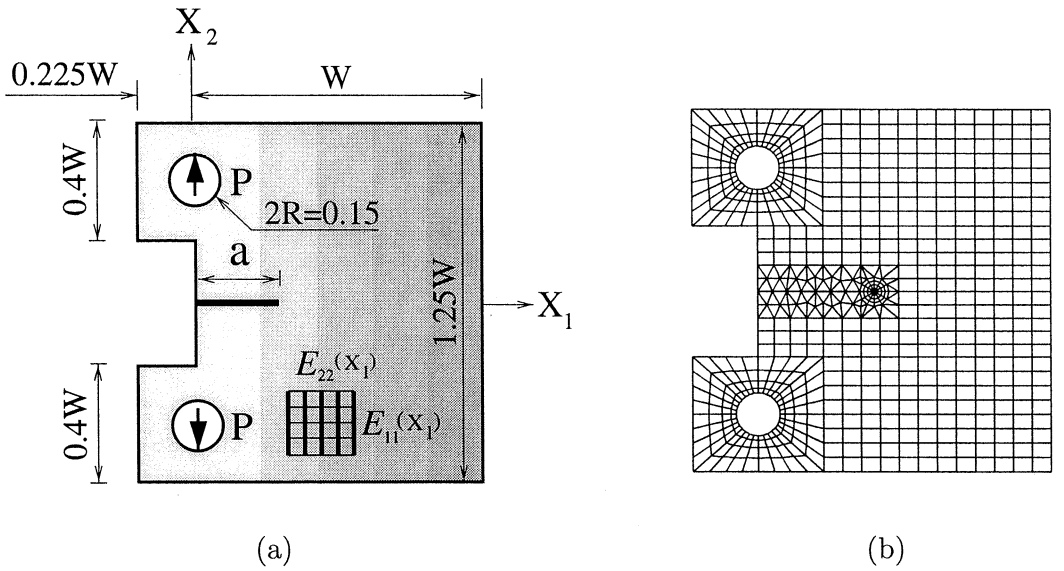

Figure 17. Example 6: compact tension (CT) specimen: (a) geometry and BCs; (b) complete finite element mesh.

T-stress decreases with the translation factor d for the range between -0.5 and 0.0, however, it increases as d increases further. For nonproportional material variations (Case 3), the T-stress decreases with the translation factor d for the range between -0.5 and -0.1, however, it increases as d increases further. Moreover, the crack tip location shows a significant influence on T-stress for all the three cases of hyperbolic-tangent material variation.

7.6. Compact tension (CT) specimen

Figure 17a shows the geometry of a CT specimen, and Figure 17b shows the complete finite mesh configuration with 12 sectors (S12) and 4 rings (R4) around the crack tip. The applied load corresponds to $P(0, \pm 0.275) = 1$. The displacement boundary condition is prescribed as $(u_1, u_2)(W, 0) = (0, 0)$ and $u_2(a, 0) = 0$. Young's moduli and shear modulus are exponential functions of X_1, while the Poisson's ratio is constant. The material properties are given by

$$\begin{aligned} &\text{For } -0.225W \le X_1 < 0,\ E_{11} = E_{11}^0,\ E_{22} = E_{22}^0, G_{12} = G_{12}^0,\ \nu_{12} = \nu_{12}^0, \\ &\text{For } 0 \le X_1 \le W,\ E_{11} = E_{11}^0 e^{\beta X_1},\ E_{22} = E_{22}^0 e^{\beta X_1}, G_{12} = G_{12}^0 e^{\beta X_1},\ \nu_{12} = \nu_{12}^0, \end{aligned} \tag{66}$$

with

$$E_{11}^0 = 1,\ E_{22}^0 = 2, G_{12}^0 = 0.5,\ \nu_{12}^0 = 0.15. \tag{67}$$

The following data are used for the FEM analysis:

$$\begin{aligned} a/W &= 0.1 \text{ to } 0.8,\ W = 1 \\ E_R = E_{11}(W)/E_{11}(0) &= E_{22}(W)/E_{22}(0) = G_{12}(W)/G_{12}(0) \\ &= \exp(\beta W) = (0.1, 0.2, 1.0, 5, 10) \\ &\text{plane stress and } 2 \times 2 \text{ Gauss quadrature.} \end{aligned} \tag{68}$$

Figure 18 shows biaxiality ratio $B = T\sqrt{\pi a}/K_I$ versus a/W ratio. The mode I SIF K_I is also evaluated by means of the interaction integral method (Kim and Paulino, 2003b). For

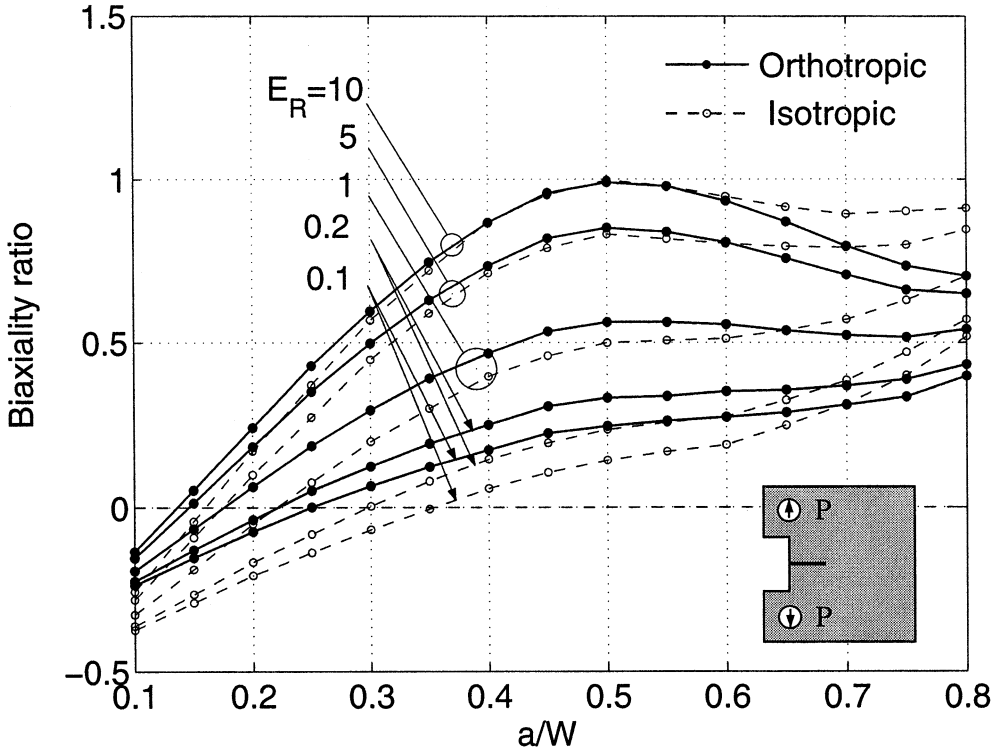

Figure 18. Example 6: Biaxiality ratio ($B = T\sqrt{\pi a}/K_I$) for a compact tension (CT) specimen. Here $E_R = E_{11}(W)/E_{11}(0) = E_{22}(W)/E_{22}(0) = G_{12}(W)/G_{12}(0) = \exp(\beta W)$.

both isotropic and orthotropic cases, as the ratio $E_R = \exp(\beta W)$ increases, the biaxiality ratio increases and the transition points for sign-change of the biaxiality ratio shift to the left. Both material orthotropy and nonhomogeneity show a significant influence on the T-stress and biaxiality ratio.

8. Concluding remarks and extensions

This paper presents a robust scheme for evaluating the T-stress by means of the interaction integral (M-integral) method considering arbitrarily oriented straight or curved cracks in two-dimensional (2D) elastic orthotropic nonhomogeneous materials. The scope of the present formulation is broad enough to cover orthotropic nonhomogeneous, orthotropic homogeneous, isotropic nonhomogeneous and isotropic homogeneous materials. This paper makes use of auxiliary fields, which are derived based on two formulations: Lekhnitskii and Stroh. As shown by Barnett and Kirchner (1997), these two formulations are equivalent, and this equivalence has also been verified in the present work both theoretically and numerically. From numerical investigations, we observe that the T-stress computed by the present method is reasonably accurate in comparison with available reference solutions, and that material orthotropy and material nonhomogeneity influences the magnitude and the sign of the T-stress.

Because SIFs and T-stress can be calculated by means of a unified approach using the interaction integral method, a potential extension of this work includes using these quantities as the basis to evaluate crack initiation angle, and develop fracture criteria in orthotropic func-

tionally graded materials (see, for example, Boone et al. (1987) for orthotropic homogeneous materials using SIF-based techniques).

Acknowledgements

We gratefully acknowledge the support from NASA-Ames, Engineering for Complex Systems Program, and the NASA-Ames Chief Engineer (Dr. Tina Panontin) through grant NAG 2-1424. We also acknowledge additional support from the National Science Foundation (NSF) under grant CMS-0115954 (Mechanics & Materials Program). In addition, we would like to thank three anonymous reviewers for their valuable comments and suggestions. Any opinions expressed herein are those of the writers and do not necessarily reflect the views of the sponsors.

References

Barnett, D.M. and Kirchner, H.O.K. (1997). A proof of the equivalence of the Stroh and Lekhnitskii sextic equations for plane anisotropic elastostatics. **76**(1), 231–239.

Betegón, C. and Hancock, J.W. (1991). Two-parameter characterization of elastic-plastic crack-tip field. *Journal of Applied Mechanics, Transactions ASME*, **58**(1), 104–110.

Boone, T.J. and Wawrzynek, P.A. and Ingraffea, A.R. (1987). Finite element modeling of fracture propagation in orthotropic materials. *Engineering Fracture Mechanics*, **26**(2), 185–201.

Budiansky, B. and Rice, J.R. (1973). Conservation laws and energy-release rates. *Journal of Applied Mechanics, Transactions ASME*, **40**(1), 201–203.

Cardew, G.E., Goldthorpe, M.R., Howard, I.C. and Kfouri, A.P. (1985). On the elastic T-term. *Fundamentals of Deformation and Fracture: Eshelby Memorial Symposium*.

Chang, J.H. and Chien, A.J. (2002). Evaluation of M-integral for anisotropic elastic media with multiple defects. *International Journal of Fracture*, **114**(3), 264–289.

Chen, C.S., Krause, R., Pettit, R.G., Banks-Sills, L. and Ingraffea, A.R. (2001). Numerical assessment of T-stress computation using a P-version finite element method. *International Journal of Fracture* **107**(2), 177–199.

Cotterell, B. and Rice, J.R. (1980). Sligthly curved or kinked cracks. *International Journal of Fracture*, **16**(2), 155–169.

Dolbow, J. and Gosz, M. (2002). On the computation of mixed-mode stress intensity factors in functionally graded materials. *International Journal of Solids and Structures*, **39**(9), 2557–2574.

Du, Z.-Z. and Hancock, J.W. (1991). The effect of non-singular stresses on crack-tip constraint. *Journal of the Mechanics and Physics of Solids* **39**(3), 555–567.

Eischen, J.W. (1987). Fracture of non-homogeneous materials. *International Journal of Fracture*, **34**(1), 3–22.

Gao, H. and Chiu, C.-H. (1992). Slightly curved or kinked cracks in anisotropic elastic solids. *International Journal of Solids and Structures*, **29**(8), 947–972.

Gu, P., and Asaro, R.J. (1997). Cracks in functionally graded materials. *International Journal of Solids and Structures*, **34**(1), 1–17.

Ilschner, B. (1996). Processing-microstructure-property relationships in graded materials. *Journal of the Mechanics and Physics of Solids*, **44**(5), 647–656.

Becker, Jr. T. L., Cannon, R.M. and Ritchie, R.O. (2001). Finite crack kinking in T-stresses in functionally graded materials. *International Journal of Solids and Structures*, **38**(32–33), 5545-5563.

Kanninen, M.F. and Popelar, C.H. (1985). *Advanced Fracture Mechanics*. Oxford University Press, New York.

Kaysser, W.A. and Ilschner, B. (1995). FGM research activities in Europe. *M.R.S. Bulletin*, **20**(1), 22–26.

Kfouri, A.P. (1986). Some evaluations of the elastic T-term using Eshelby's method. *International Journal of Fracture*, **30**(4), 301–315.

Kim, J.-H. (2003). Mixed-mode crack propagation in functionally graded materials. *Ph.D. Thesis*, University of Illinois at Urbana-Champaign.

Kim, J.-H. and Paulino, G.H. (2002a). Finite element evaluation of mixed-mode stress intensity factors in functionally graded materials. *International Journal for Numerical Methods in Engineering*, **53**(8), 1903–1935.

Kim, J.-H. and Paulino, G.H. (2002b). Isoparametric graded finite elements for nonhomogeneous isotropic and orthotropic materials. *Journal of Applied Mechanics, Transactions ASME*, **69**(4), 502–514.

Kim, J.-H. and Paulino, G.H. (2002c). Mixed-mode fracture of orthotropic functionally graded materials using finite elements and the modified crack closure method. *Engineering Fracture Mechanics*, **69**(14–16), 1557–1586.

Kim, J.-H. and Paulino, G.H. (2003a). An accurate scheme for mixed-mode fracture analysis of functionally graded materials using the interaction integral and micromechanics models. *International Journal for Numerical Methods in Engineering*, **58**(10), 1457–1497.

Kim, J.-H. and Paulino, G.H. (2003b). The interaction integral for fracture of orthotropic functionally graded materials: Evaluation of stress intensity factors. *International Journal of Solids and Structures*, **40**(15), 3967–4001.

Kim, J.-H. and Paulino, G.H. (2003c). Mixed-mode J-integral formulation and implementation using graded finite elements for fracture analysis of nonhomogeneous orthotropic materials. *Mechanics of Materials*, **35**(1–2), 107–128.

Kim, J.-H. and Paulino, G.H. (2003d). T-stress, mixed-mode stress intensity factors, and crack initiation angles in functionally graded materials: A unified approach using the interaction integral method. *Computer Methods in Applied Mechanics and Engineering*, **192**(11–12), 1463–1494.

Knowles, J.K. and Sternberg, E. (1972). On a class of conservation laws in linearized and finite elastostatics. *Archive for Rational Mechanics and Analysis*, **44**(2), 187–211.

Larsson, S.G. and Carlson, A.J. (1973). Influence of non-singular stress terms and specimen geometry on small-scale yielding at crack tips in elastic-plastic materials. *Journal of the Mechanics and Physics of Solids*, **21**(4), 263–277.

Leevers, P.S. and Radon, J.C.D. (1982). Inherent stress biaxiality in various fracture specimen. *International Journal of Fracture*, **19**(4), 311–325.

Lekhnitskii, S.G. (1968). *Anisotropic plates*. Gordon and Breach Science Publishers, New York.

Miyamoto, Y., Kaysser, W.A., Rabin, B.H., Kawasaki, A. and Ford, R.G. (1999). *Functionally Graded Materials: Design, Processing and Applications*. Kluwer Academic Publishers, Dordrecht.

Muskhelishvili, N.I. (1953). *Some Basic Problems of the Mathematical Theory of Elasticity*. Noordhoff Ltd., Holland.

O'Dowd, N.P. and Shih, C.F. (1991). Family of crack-tip fields characterized by a triaxiality parameter - I. structure of fields. *Journal of the Mechanics and Physics of Solids*, **39**(8), 989–1015.

O'Dowd, N.P. and Shih, C.F. (1992). Family of crack-tip fields characterized by a triaxiality parameter - II. fracture applications. *Journal of the Mechanics and Physics of Solids*, **40**(5), 939–963.

O'Dowd, N.P., Shih, C.F. and Dodds Jr., R.H. (1995). The role of geometry and crack growth on constraint and implications for ductile/brittle fracture. In *Constraint Effects in Fracture Theory and Applications*, volume 2 of *ASTM STP 1244*, pp. 134–159. American Society for Testing and Materials.

Paulino, G.H., Jin, Z.H. and Dodds Jr., R.H. (2003). Failure of functionally graded materials. In B. Karihaloo and W.G. Knauss, editors, *Comprehensive Structural Integrity*, volume 2, Chapter 13, pp. 607–644. Elsevier Science.

Paulino, G.H. and Kim, J.-H. (2004). A new approach to compute T-stress in functionally graded materials by means of the interaction integral method. *Engineering Fracture Mechanics*, in press.

Raju, I.S. and Shivakumar, K.N. (1990). An equivalent domain integral method in the two-dimensional analysis of mixed mode crack problems. *Engineering Fracture Mechanics*, **37**(4), 707–725.

Rice, J.R. (1968). A path-independent integral and the approximate analysis of strain concentration by notches and cracks. *Journal of Applied Mechanics, Transactions ASME*, **35**(2), 379–386.

Sampath, S., Herman, H., Shimoda, N. and Saito, T. (1995). Thermal spray processing of FGMs. *M.R.S. Bulletin*, **20**(1), 27–31.

Shih, G.C., Paris, P.C. and Irwin, G.R. (1965). On cracks in rectilinearly anisotropic bodies. *International Journal of Fracture Mechanics*, **1**(2), 1989–203.

Sladek, J., Sladek, V. and Fedelinski, P. (1997). Contour integrals for mixed-mode crack analysis: effect of nonsingular terms. *Theoretical and Applied Fracture Mechanics*, **27**(2), 115–127.

Smith, D.J., Ayatollahi, M.R. and Pavier, M.J. (2001). The role of T-stress in brittle fracture for linear elastic materials under mixed-mode loading. *Fatigue and Fracture of Engineering Materials and Structures*, **24**(2), 137–150.

Suresh, S. and Mortensen, A. (1998). *Fundamentals of Functionally Graded Materials*. IOM Communications Ltd., London.

Ting, C.T.C. (1996). *Anisotropic Elasticity: Theory and Applications*. Oxford University Press, Oxford.

Tokita, M. (1999). Development of large-size ceramic metal bulk FGM fabricated by spark plasma sintering. *Materials Science Forum*, **308–311**, 83–88.

Ueda, Y., Ikeda, K., Yao, T. and Aoki, M. (1983). Characteristics of brittle failure under general combined modes including those under bi-axial tensile loads. *Engineering Fracture Mechanics*, **18**(6), 1131–1158.

Wawrzynek, P.A. (1987). Interactive finite element analysis of fracture process: an integrated approach. *M.S. Thesis, Cornell University*.

Wawrzynek, P.A. and Ingraffea, A.R. (1991). Discrete modeling of crack propagtion: theorectical aspects and implementation issus in two and three dimensions. *Report 91-5, School of Civil Engineering and Environmental Engineering, Cornell University*.

Williams, J.G. and Ewing, P.D. (1972). Fracture under complex stress - the angled crack problem. *International Journal of Fracture*, **8**(4), 441–416.

Williams, J.G. (1957). On the stress distribution at the base of a stationary crack. *Journal of Applied Mechanics, Transactions ASME*, **24**(1), 109–114.

Yang, S. and Yuan, F.G. (2000a). Determination and representation of the stress coefficient terms by path-independent integrals in anisotropic cracked solids. *International Journal of Fracture*, **101**(4), 291–319.

Yang, S. and Yuan, F.G. (2000b). Kinked crack in anisotropic bodies. *International Journal of Solids and Structures*, **37**(45), 6635–6682.

Appendix A. derivatives of auxiliary displacements in the Lekhnitskii formalism

The stress-strain relationship, with respect to polar coordinates (r, ϕ), leads to

$$\varepsilon_{rr}^{aux} = \frac{\partial u_r}{\partial r} = a'_{11}(\phi)\frac{A\cos\phi + B\sin\phi}{r\mathcal{F}(\phi)}, \tag{69}$$

$$\varepsilon_{\phi\phi}^{aux} = \frac{u_r}{r} + \frac{\partial u_\phi}{r\partial\phi} = a'_{12}(\phi)\frac{A\cos\phi + B\sin\phi}{r\mathcal{F}(\phi)}, \tag{70}$$

$$\varepsilon_{r\phi}^{aux} = \frac{1}{2}\left(\frac{\partial u_r}{r\partial\phi} + \frac{\partial u_\phi}{\partial r} - \frac{u_\phi}{r}\right) = 0, \tag{71}$$

where, for the case of material orthotropy directions aligned with the global coordinates,

$$\begin{aligned} a'_{11}(\phi) &= \mathcal{F}(\phi) = a_{11}^{\text{tip}}\cos^4\phi + (2a_{12}^{\text{tip}} + a_{66}^{\text{tip}})\sin^2\phi\cos^2\phi + a_{22}^{\text{tip}}\sin^4\phi, \\ a'_{12}(\phi) &= a_{12}^{\text{tip}} + (a_{11}^{\text{tip}} + a_{22}^{\text{tip}} - 2a_{12}^{\text{tip}} - a_{66}^{\text{tip}})\sin^2\phi\cos^2\phi. \end{aligned} \tag{72}$$

Integration of Equation (69) with respect to r leads to

$$u_r = (A\cos\phi + B\sin\phi)\ln r + g(\phi), \tag{73}$$

where $g(\phi)$ is the unknown function of ϕ. Substitution of Equation (73) into Equation (70) yields

$$u_\phi = \int_\phi a'_{12}(\phi)\frac{A\cos\phi + B\sin\phi}{\mathcal{F}(\phi)}\,d\phi - \ln r\int_\phi (A\cos\phi + B\sin\phi)\,d\phi - \int_\phi g(\phi)\,d\phi + h(r), \tag{74}$$

where the first indefinite integral is not integrable analytically and $h(r)$ is the unknown function of r. By substituting Equations (73) and (74) into Equation (71), one obtains the following condition

$$r\frac{\partial h(r)}{\partial r} - h(r) = 0, \tag{75}$$

which yields $h(r) = Cr$ with a constant C. Differentiations of u_r of Equation (73) and u_ϕ of Equation (74) with respect to r are

$$\begin{aligned} \frac{\partial u_r}{\partial r} &= \frac{1}{r}(A\cos\phi + B\sin\phi) \\ \frac{\partial u_\phi}{\partial r} &= -\frac{1}{r}(A\sin\phi - B\cos\phi) + C, \end{aligned} \tag{76}$$

where $C = 0$ because $\partial u_1/\partial r$, $\partial u_r/\partial r$, and $\partial u_\phi/\partial r$ must have a separable form of $(1/r) \times p(\phi)$. Then

$$\frac{\partial u_1}{\partial r} = \frac{\partial u_r}{\partial r}\cos\phi - \frac{\partial u_\phi}{\partial r}\sin\phi = \frac{A}{r}. \tag{77}$$

Using the chain rule of differentiation and Equation (77), one writes

$$u_{1,1} = \frac{\partial u_1}{\partial r}\frac{\partial r}{\partial X_1} + \frac{\partial u_1}{\partial \phi}\frac{\partial \phi}{\partial X_1} = (a_{11}^{\text{tip}}\cos^2\phi + a_{12}^{\text{tip}}\sin^2\phi)\frac{A\cos\phi + B\sin\phi}{r\mathcal{F}(\phi)}, \tag{78}$$

with

$$\begin{aligned} &\frac{\partial r}{\partial X_1} = \cos\phi, \quad \frac{\partial r}{\partial X_2} = \sin\phi, \\ &\frac{\partial \phi}{\partial X_1} = \frac{-\sin\phi}{r}, \quad \frac{\partial \phi}{\partial X_2} = \frac{\cos\phi}{r}. \end{aligned} \tag{79}$$

By means of the same procedure above, one obtains $u_{2,2}$ as

$$u_{2,2} = \frac{\partial u_2}{\partial r}\frac{\partial r}{\partial X_2} + \frac{\partial u_2}{\partial \phi}\frac{\partial \phi}{\partial X_2} = (a_{12}^{\text{tip}}\cos^2\phi + a_{22}^{\text{tip}}\sin^2\phi)\frac{A\cos\phi + B\sin\phi}{r\mathcal{F}(\phi)}. \tag{80}$$

Solution of Equation (78) for the unknown $\partial u_1/\partial\phi$ leads to

$$\frac{\partial u_1}{\partial \phi} = -\frac{1}{\mathcal{F}(\phi)}(A\mathcal{H}_1(\phi) + B\mathcal{H}_2(\phi)), \tag{81}$$

where $\mathcal{H}_1(\phi)$ and $\mathcal{H}_2(\phi)$ are given by Equation (15). Using $\partial u_1/\partial r$ (Equation (77)) and $\partial u_1/\partial\phi$ (Equation (81)), one obtains $u_{1,2}$ and $u_{2,1}$ as follows:

$$\begin{aligned} u_{1,2} &= \frac{\partial u_1}{\partial r}\frac{\partial r}{\partial X_2} + \frac{\partial u_1}{\partial \phi}\frac{\partial \phi}{\partial X_2} \\ u_{2,1} &= 2a_{66}^{\text{tip}}\sigma_{12}^{aux} - u_{1,2}. \end{aligned} \tag{82}$$

The expressions for derivatives of displacements $u_{i,j}$ $(i, j = 1, 2)$ are given in Equation (14).

Appendix B. Stroh Formalism

Let's consider an orthotropic linear elastic body in two dimensional fields. According to the Stroh formalism, the displacement vector $\boldsymbol{u}$ and the stress function vector $\boldsymbol{\Phi}$ are given by (Ting, 1996)

$$\boldsymbol{u} = \mathrm{Re}\,[\boldsymbol{A}\ \boldsymbol{f}(z)\ \boldsymbol{d}], \quad \boldsymbol{\Phi} = \mathrm{Re}\,[\boldsymbol{B}\ \boldsymbol{f}(z)\ \boldsymbol{d}], \tag{83}$$

where

$$\begin{gathered}\sigma_{i1} = -\Phi_{i,2}, \ \ \sigma_{i2} = \Phi_{i,1} \\ \boldsymbol{A} = [\boldsymbol{a}_1, \boldsymbol{a}_2], \quad \boldsymbol{B} = [\boldsymbol{b}_1, \boldsymbol{b}_2], \\ \boldsymbol{f}(z) = \mathrm{diag}[f(z_1), f(z_2)], \ \ z_k = x_1 + \mu_k x_2, \ \ \mathrm{Im}[\mu_k] > 0 \ \ (k = 1, 2),\end{gathered} \tag{84}$$

in which $\boldsymbol{f}(z)$ is a diagonal matrix of an arbitrary complex function; $\boldsymbol{d}$ is an unknown complex constant vector; $\boldsymbol{\mu}_k$, $\boldsymbol{a}_k$ and $\boldsymbol{b}_k$ are the Stroh eigenvalues and eigenvectors, respectively, which are functions of material parameters. These are obtained by the following eigenvalue problem (Ting, 1996):

$$\boldsymbol{N}\boldsymbol{p} = \mu\boldsymbol{p}, \tag{85}$$

where

$$\begin{gathered}\boldsymbol{N} = \begin{bmatrix} \boldsymbol{N}_1 & \boldsymbol{N}_2 \\ \boldsymbol{N}_3 & \boldsymbol{N}_1^T \end{bmatrix}, \boldsymbol{p} = \begin{bmatrix} \boldsymbol{a} \\ \boldsymbol{b} \end{bmatrix}, \\ \boldsymbol{N}_1 = -\boldsymbol{T}^{-1}\boldsymbol{R}^T, \ \boldsymbol{N}_2 = \boldsymbol{T}^{-1}, \ \boldsymbol{N}_3 = \boldsymbol{R}\boldsymbol{T}^{-1}\boldsymbol{R}^T - \boldsymbol{Q},\end{gathered} \tag{86}$$

in which $\boldsymbol{Q}$, $\boldsymbol{R}$ and $\boldsymbol{T}$ are 2×2 matrices given by:

$$Q_{ij} = C_{i1j1}, \ \ R_{ij} = C_{i1j2}, \ \ T_{ij} = C_{i2j2} \ \text{ with } \ \sigma_{pq} = C_{pqst}\varepsilon_{st}. \tag{87}$$

Since the 4×4 matrix $\boldsymbol{N}$ is not symmetric and the strain energy is positive definite, there exist two pairs of complex conjugates for μ as follows:

$$\mu_k = \overline{\mu_k}, \ \ \boldsymbol{a}_{k+2} = \overline{\boldsymbol{a}}_k, \ \ \boldsymbol{b}_{k+2} = \overline{\boldsymbol{b}}_k, \ \ (k = 1, 2). \tag{88}$$

Because $\boldsymbol{N}$ is not symmetric, the $\boldsymbol{p}$ in Equation (85) is a right eigenvector. The right eigenvector $\boldsymbol{q}$ satisfies the following eigen-relation (Ting, 1996):

$$\boldsymbol{N}^T\boldsymbol{q} = \mu\boldsymbol{q} \tag{89}$$

and is given by

$$\boldsymbol{q} = \begin{bmatrix} \boldsymbol{b} \\ \boldsymbol{a} \end{bmatrix}. \tag{90}$$

For different eigenvalues ($\mu_k \neq \mu_l$) the left and right eigenvectors are orthogonal to each other, i.e.

$$\boldsymbol{q}_k\boldsymbol{p}_l = 0. \tag{91}$$

Assuming that μ_k are distinct, we normalize p_k such that

$$\boldsymbol{q}_k\boldsymbol{p}_l = \delta_{kl} \ \text{ or } \ \boldsymbol{b}_k^T\boldsymbol{a}_l + \boldsymbol{a}_k^T\boldsymbol{b}_l = \delta_{kl}, \tag{92}$$

where δ_{kl} is the Kronecker delta. Combining Equations (91) with (92) leads to

$$\begin{bmatrix} \boldsymbol{B}^T & \boldsymbol{A}^T \\ \overline{\boldsymbol{B}}^T & \overline{\boldsymbol{A}}^T \end{bmatrix} \begin{bmatrix} \boldsymbol{A} & \overline{\boldsymbol{A}} \\ \boldsymbol{B} & \overline{\boldsymbol{B}} \end{bmatrix} = \begin{bmatrix} \boldsymbol{I} & \boldsymbol{0} \\ \boldsymbol{0} & \boldsymbol{I} \end{bmatrix}, \tag{93}$$

where $\boldsymbol{I}$ is the 2×2 identity matrix. The 4×4 matrices on the left of Equation (93) are the inverses to each other. Thus

$$\begin{bmatrix} \boldsymbol{A} & \overline{\boldsymbol{A}} \\ \boldsymbol{B} & \overline{\boldsymbol{B}} \end{bmatrix} \begin{bmatrix} \boldsymbol{B}^T & \boldsymbol{A}^T \\ \overline{\boldsymbol{B}}^T & \overline{\boldsymbol{A}}^T \end{bmatrix} = \begin{bmatrix} \boldsymbol{I} & \boldsymbol{0} \\ \boldsymbol{0} & \boldsymbol{I} \end{bmatrix}, \tag{94}$$

or

$$\begin{aligned} &\boldsymbol{A}\boldsymbol{B}^T + \overline{\boldsymbol{A}}\,\overline{\boldsymbol{B}}^T = \boldsymbol{I} = \boldsymbol{B}\boldsymbol{A}^T + \overline{\boldsymbol{B}}\,\overline{\boldsymbol{A}}^T \\ &\boldsymbol{A}\boldsymbol{A}^T + \overline{\boldsymbol{A}}\,\overline{\boldsymbol{A}}^T = \boldsymbol{0} = \boldsymbol{B}\boldsymbol{B}^T + \overline{\boldsymbol{B}}\,\overline{\boldsymbol{B}}^T. \end{aligned} \tag{95}$$

Equation (95) shows that the real part of $\boldsymbol{A}\boldsymbol{B}^T$ is $\boldsymbol{I}/2$, and $\boldsymbol{A}\boldsymbol{A}^T$ and $\boldsymbol{B}\boldsymbol{B}^T$ are purely imaginary. Thus the three real matrices are defined as follows (Ting, 1996):

$$\boldsymbol{S} = i(2\boldsymbol{A}\boldsymbol{B}^T - \boldsymbol{I}),\ \boldsymbol{H} = 2i\,\boldsymbol{A}\boldsymbol{A}^T,\ \boldsymbol{L} = -2i\,\boldsymbol{B}\boldsymbol{B}^T. \tag{96}$$

Appendix C. Nomenclature

a	half crack length
a_{ij}	contracted notation of the compliance tensor for plane stress; i = 1,2,6; j = 1,2,6
a_{ij}^{tip}	a_{ij} evaluated at the crack tip location; i, j = 1,2,6
$\boldsymbol{A}$	a 2×2 complex matrix
b_{ij}	contracted notation of the compliance tensor for plane strain; i = 1,2,6; $j = 1, 2, 6$
b_{ij}^{tip}	b_{ij} evaluated at the crack tip location; $i, j = 1, 2, 6$
$\boldsymbol{B}$	a 2×2 complex matrix
C_{ijkl}	constitutive tensor for anisotropic materials; $i, j, k, l = 1, 2, 3$
d	translation factor in hyperbolic-tangent function
e	natural logarithm base, $e = 2.71828182\ldots$
E_{11}, E_{22}	Young's moduli with respect to the principal axes of orthotropy
E_{11}^0, E_{22}^0	Young's moduli E_{11}, E_{22} evaluated at the origin
f	a point force
$\boldsymbol{f}$	an arbitrary complex function
G_{12}	shear modulus in orthotropic materials
G_{12}^0	shear modulus G_{12} evaluated at the origin
h_1, h_2	dimensions of the beam specimen
H	length of material gradation
$\boldsymbol{I}$	the 2×2 identity matrix
$\boldsymbol{H}$	a 2×2 real matrix
$\mathcal{H}$	contour integral
Im	imaginary part of the complex function
J	path-independent J-integral for the actual field
J^{aux}	J-integral for the auxiliary field
J^s	J-integral for the superimposed fields (actual plus auxiliary)
K_I	mode I stress intensity factor
K_{II}	mode II stress intensity factor
L	length of a plate
$\boldsymbol{L}$	a 2×2 real matrix
M	interaction integral (M-integral)
$\boldsymbol{N}$	a 4×4 complex matrix
$\boldsymbol{N}_3$	a 2×2 complex matrix
m_i, n_i	unit normal vectors on the contour of the domain integral

Nomenclature (Continued)

p_k	coefficients of the asymptotic displacements for orthotropic materials; $k = 1, 2$
q_k	coefficients of the asymptotic displacements for orthotropic materials; $k = 1, 2$
q	weight function in the domain integral
$\boldsymbol{Q}$	a 2×2 real matrix
r	radial direction in polar coordinates
$\boldsymbol{R}$	a 2×2 real matrix
Re	real part of the complex function
$\boldsymbol{S}$	a 2×2 real matrix
$\boldsymbol{T}$	a 2×2 real matrix
T	T-stress
u_i	displacements for the actual field; $i = 1, 2$
u_i^{aux}	displacements for the auxiliary field; $i = 1, 2$
$\boldsymbol{u}$	2×2 displacement vector
$\boldsymbol{u}^{aux}$	2×2 auxiliary displacement vector
W	width of a plate
$\mathcal{W}$	strain energy density
$\mathcal{W}^{aux}$	strain energy density for the auxiliary field
x_i	local Cartesian coordinates; $i = 1, 2$
X_i	global Cartesian coordinates; $i = 1, 2$
z_k	complex variable, $z_k = x_k + iy_k$; $k = 1, 2$
α	material nonhomogeneity parameter for gradation of E_{11}
α_k	the real part of μ_k; $k = 1, 2$
β	material nonhomogeneity parameter for gradation of E_{22}
β_k	the imaginary part of μ_k; $k = 1, 2$
γ	material nonhomogeneity parameter for gradation of G_{12}
Γ	contour for J and M integrals
Γ_0	outer contour
Γ_s	inner contour
Γ^+	contour along the upper crack face
Γ^-	contour along the lower crack face
δ_{ij}	Kronecker delta; $i, j = 1, 2$
ε_k	contracted notation of ϵ_{ij}; $k = 1, \ldots, 6$
ε_{ij}	strains for the actual fields; $i = 1, 2, 3$; $j = 1, 2, 3$
μ_k	roots of the characteristic equation; $k = 1, 2$
μ_k^{tip}	μ_k evaluated at the crack tip location; $k = 1, 2$
$\overline{\mu}_k$	complex conjugate of μ_k; $k = 1, 2$
ν_{ij}	Poisson's ratio representing the response in direction j due to loading in direction i
σ_k	contracted notation of σ_{ij}; $k = 1, \ldots, 6$
σ_{ij}	stresses for the actual fields; i=1,2,3; $j = 1, 2, 3$
σ_{ij}^{aux}	stresses for the auxiliary fields; $i = 1, 2, 3$; $j = 1, 2, 3$
ϕ	angular direction in polar coordinates with respect to the global Cartesian coordinates
Φ	stress function vector
ω	angular direction in polar coordinates with respect to the local Cartesian coordinates